Development and Certification of NIST Standard Reference Materials for Powder Diffraction

James P. Cline

David Black, Donald Windover
Robert B. Von Dreele[1], Ryan Winburn[2],
Peter W. Stephens[3] and James J. Filliben
& Albert Henins

National Institute of Standards and Technology
Gaithersburg MD, USA

[1]Argonne National Laboratory
Argonne, IL

[2]Minot State University
Minot, ND

[3]State University of New York at Stony Brook
Stony Brook, NY

Robert W. Cheary **Richard D. Deslattes**

NIST
National Institute of Standards and Technology
U.S. Department of Commerce

Calibration of Diffraction Line Position

Qualitative phase analyses:

Improved performance of search/match algorithms

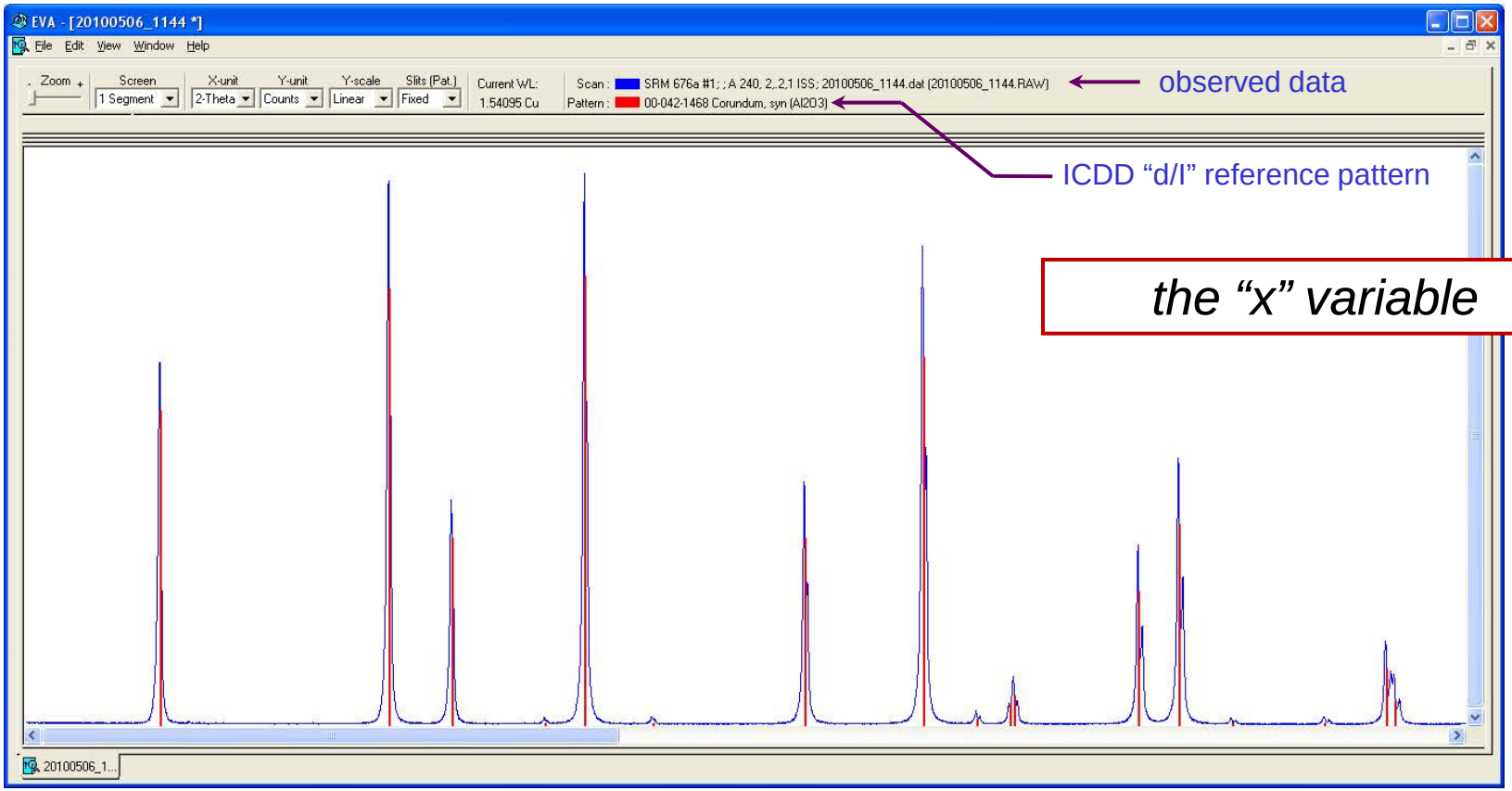

Intensity (arb units)

Two Theta

Calibration for Instrument Response

SRM 1976b: Suitable laboratory diffractometers using conventional data analysis methods

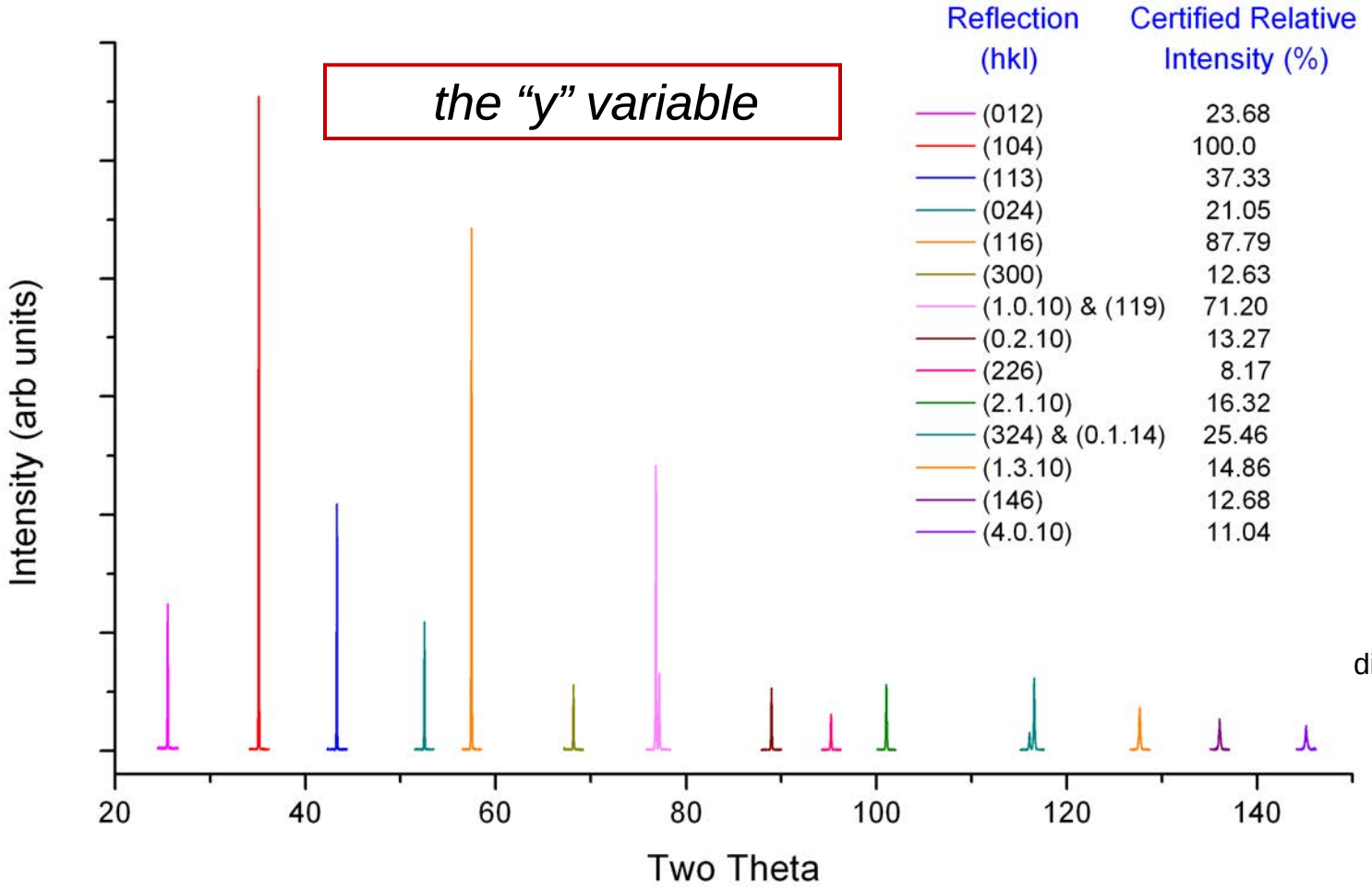

Reflection (hkl)	Certified Relative Intensity (%)
(012)	23.68
(104)	100.0
(113)	37.33
(024)	21.05
(116)	87.79
(300)	12.63
(1.0.10) & (119)	71.20
(0.2.10)	13.27
(226)	8.17
(2.1.10)	16.32
(324) & (0.1.14)	25.46
(1.3.10)	14.86
(146)	12.68
(4.0.10)	11.04

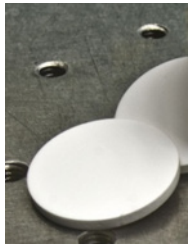

Sintered Al_2O_3 discs of SRM 1976b

Quantitative Phase Analyses

SRM 676a, alumina powder,
certified with respect to absolute phase purity

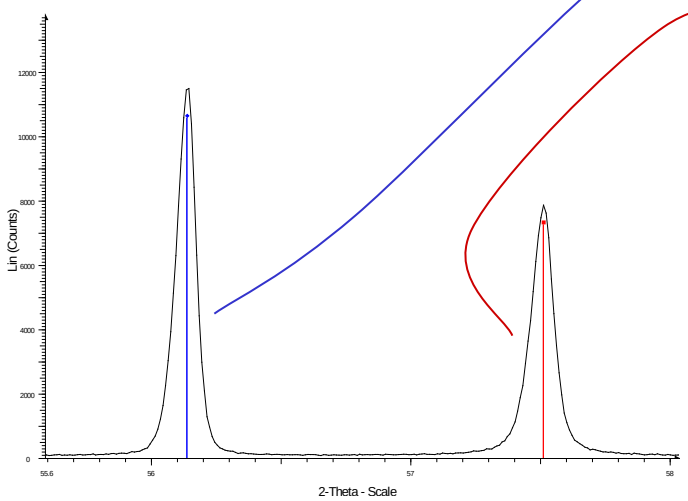

$$\frac{I_\alpha}{I_s}\left(\frac{I_{js}^{rel}}{I_{i\alpha}^{rel}}\right) RIR_{\alpha,s} = \frac{X_\alpha}{X_s}$$

Reference Intensity Ratio, RIR, (Internal Standard) Method

I/Ic, the **RIR** of a given phase relative to Al_2O_3 (corundum), Parameter included in ICDD database

Boundary of any crystalline solid will include an amorphous component
Ultimate measurement issue: Crystalline phase purity

Rietveld Analysis of Powder Diffraction Data

Rigorous modeling of all aspects of the diffraction experiment for crystal structure analysis

Refinement of SRM 660b LaB_6

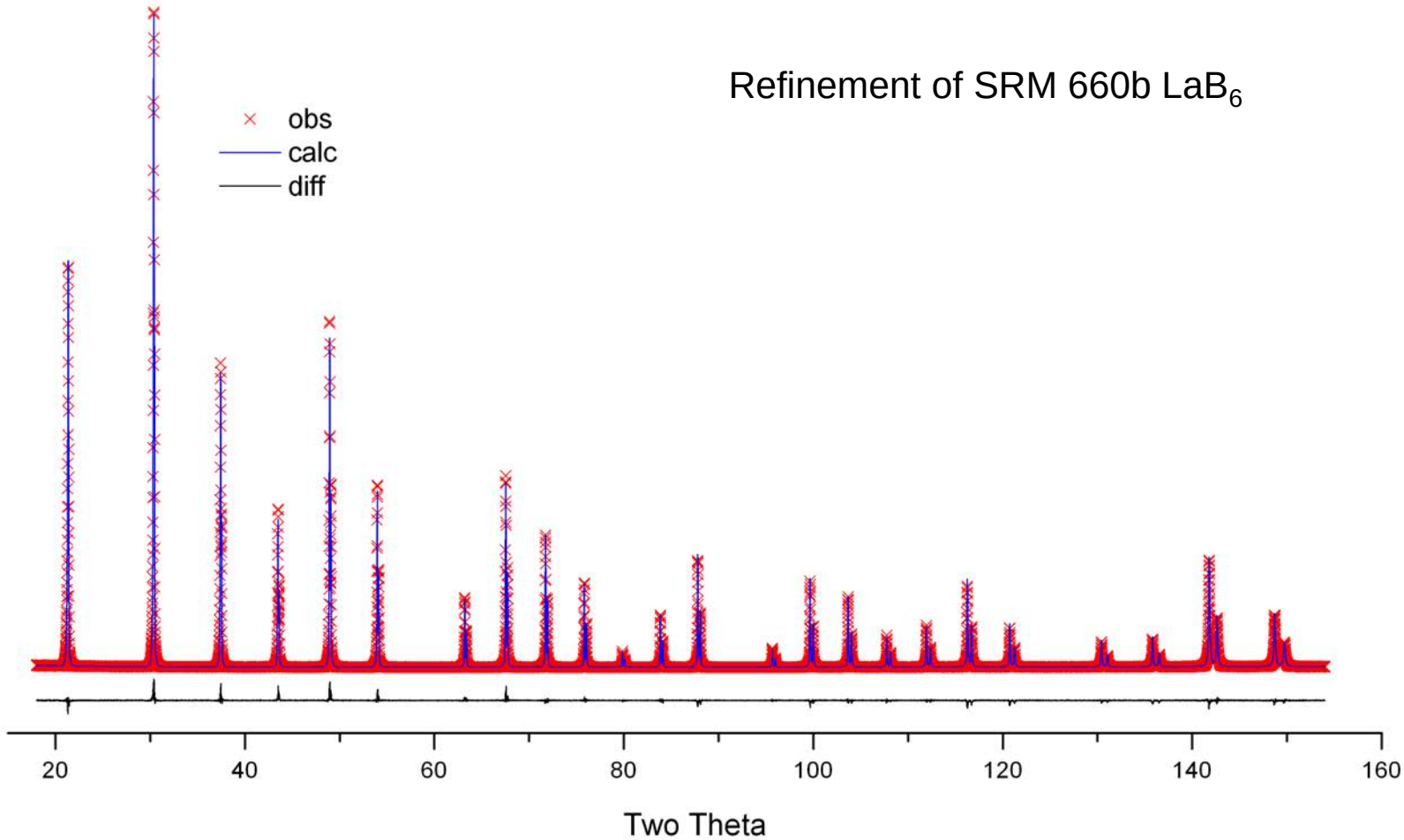

Microstructure Analysis via Powder Diffraction

Crystallite size and lattice defect induced broadening of diffraction profiles

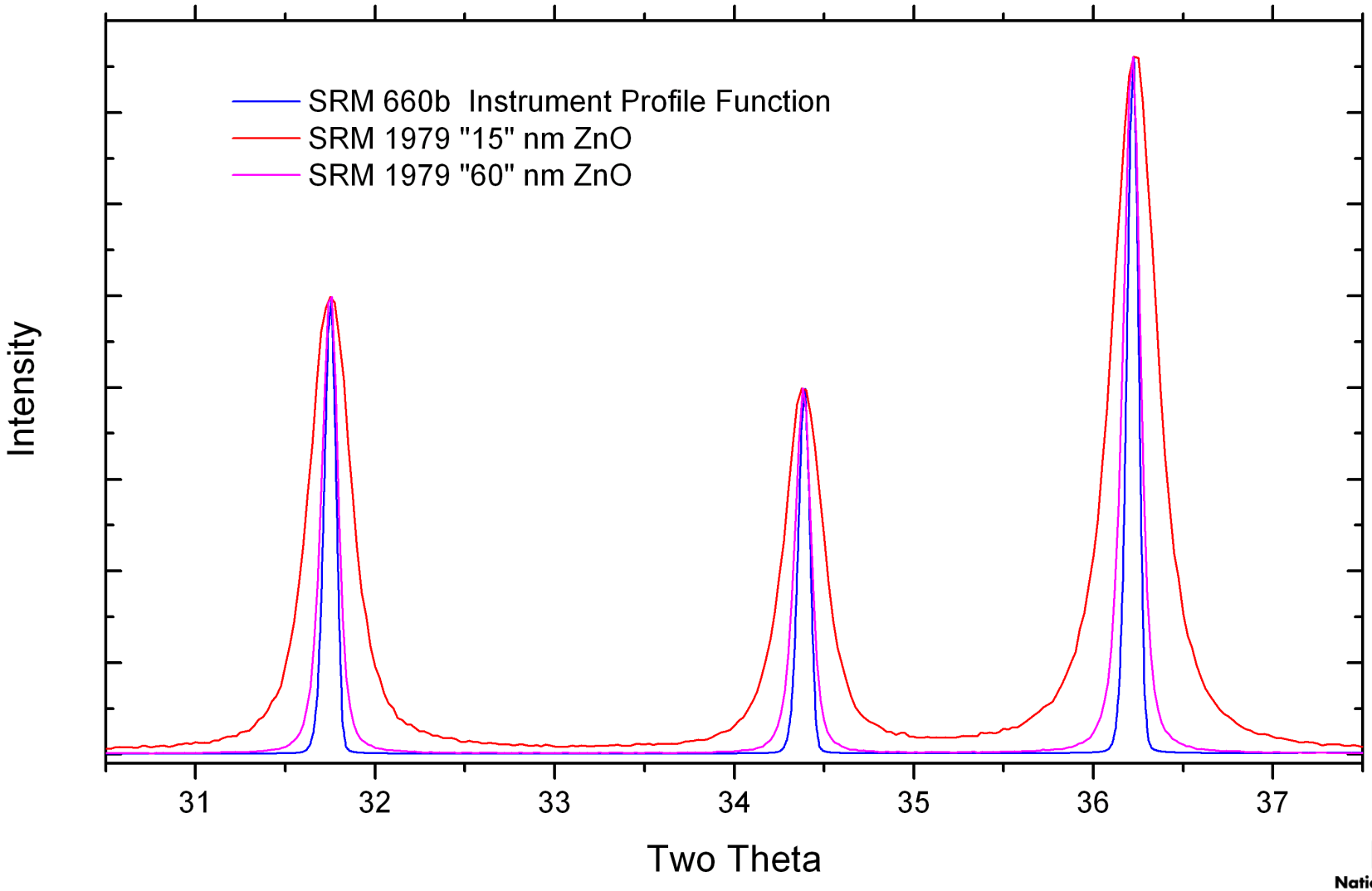

Certification of NIST Diffraction SRMs

A technical approach with four primary facets

Calibration Artifact

- ***Materials*** – Stable, non-toxic, well-characterized, homogeneous, large feedstock volumes, with microstructures optimized for diffraction properties
- ***Structure*** – Useful, easily modeled diffraction features for instrument calibration

Instrumentation & Data Collection

- ***Instrumentation*** – Three NIST- constructed gizmos, angle-encoded, capable of SI traceable measurements
- ***Instrument Response*** – Instrument performance validated using NIST SRMs

Theory & Data Analysis

- ***Theory*** – Fundamental Parameters Approach to model instrument profile function and sample microstructure
- ***Model Selection*** – Independent evaluation of IPF parameters and feedstock character

Virtues and use of SRMs

- ***Instrumentation*** – Virtues and drawbacks of various optical geometries
- ***Data Analysis Methods*** – Cost / benefit analysis of complex vs. simple methods

NIST SRMs for X-ray Wavelength Metrology

SRM	Material / Format	Diffraction Application	Unit Size (g)
640d	Silicon Powder	Line Position & Line Profile	7.5
675	Mica Powder	Line Position, Low 2θ	7.5
2000	Silicon (100) Wafer with SiGe Epilayer	High-Resolution Line Position & Reflectometry	25 mm square
660b	LaB_6 Powder	Line Position & Line Profile	6
1979	ZnO Powders	Line Profile, 20 nm & 70 nm	3
1976b	Sintered Alumina Plate	Instrument Response	2.5 cm disc
676a	Alumina (corundum) Powder	Quantitative Analysis	20
674b	Powder Set: ZnO, TiO_2, CeO_2, & Cr_2O_3	Quantitative Analysis	10 (each)
1878a	Respirable Quartz Powder	Quantitative Analysis	5
1879a	Respirable Cristobalite Powder	Quantitative Analysis	5
656	Silicon Nitride: α & β Powders	Quantitative Analysis	10 (each)

SI Traceability in Certification of Diffraction SRMs

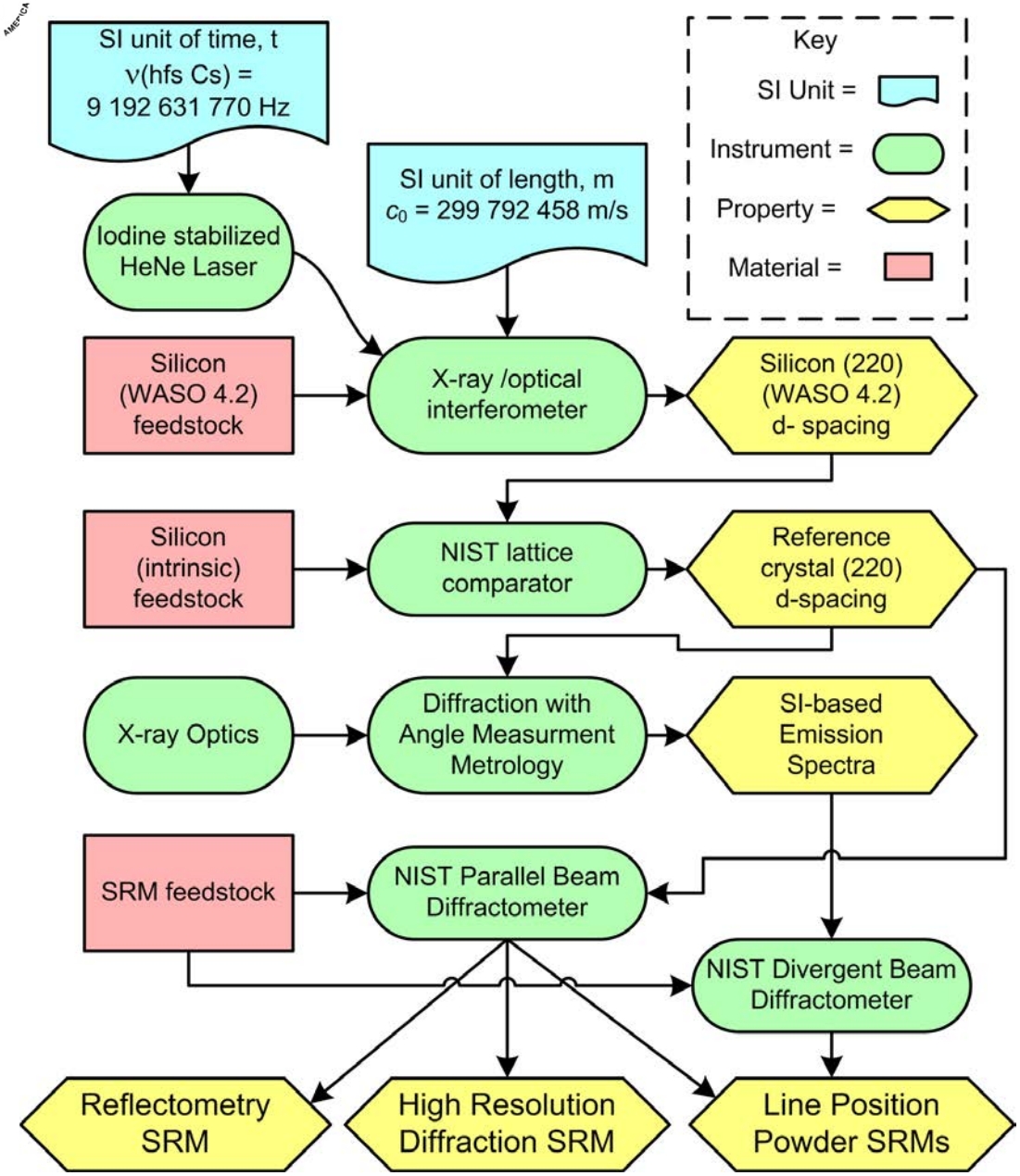

$$\lambda = 2d \sin \theta$$

Angle metrology

Parallel Beam Diffractometer (PBD)

SI traceability / accuracy in wavelength and lattice parameter measurement

Measurement capability in HRXRD, XRR, and powder diffraction

Interchangeable optics and sample stages

Vertical axes, concentrically mounted Huber 430 rotation stages

Heidenhain RON 905 optical encoders on primary axes

Short and long range encoder calibration

SI-traceable reference crystals

Located in temperature controlled environment ≈ ±0.02° C

SI Traceable Measurement of Lattice Parameters on Powders with PBD

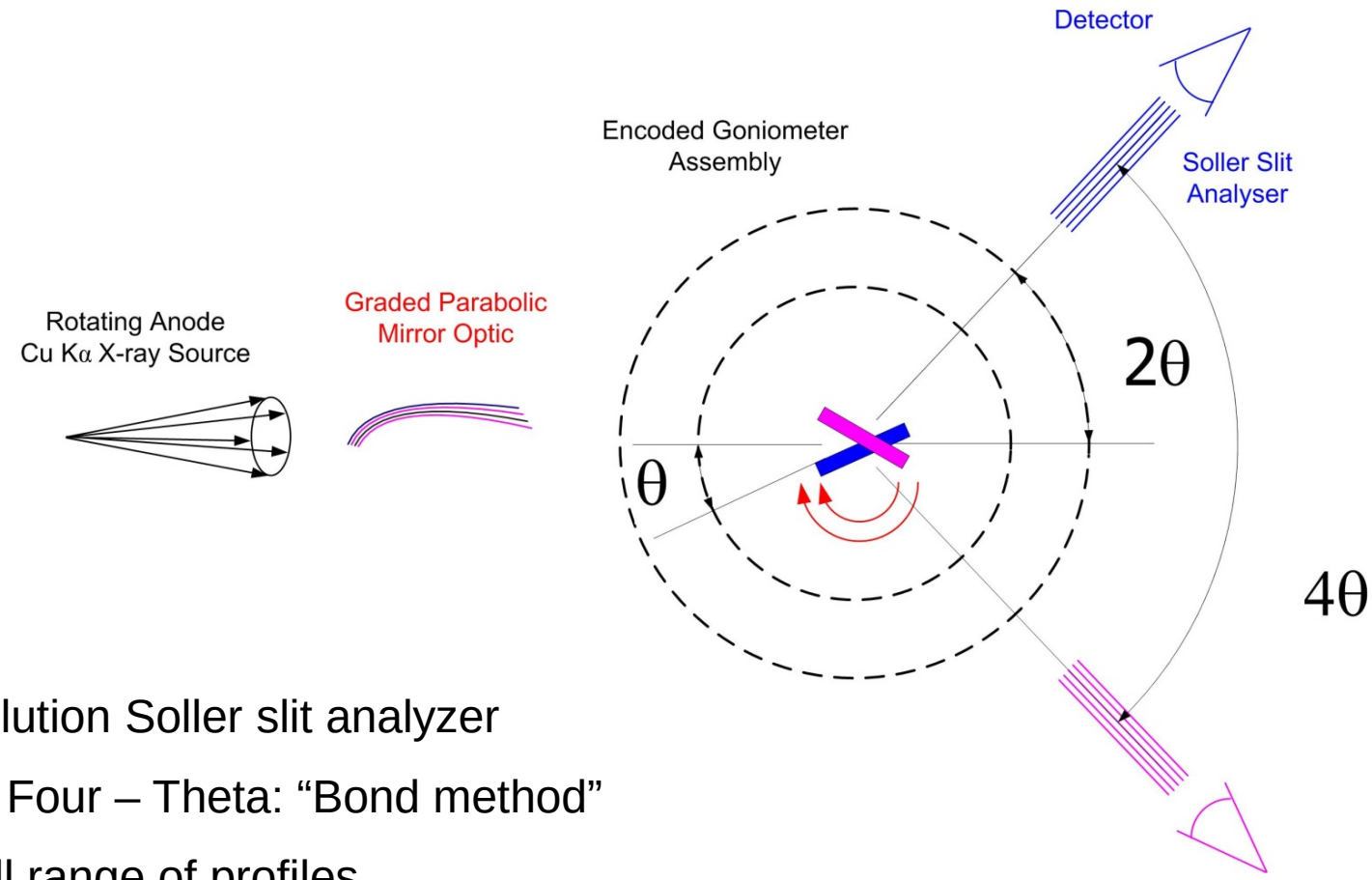

High-resolution Soller slit analyzer

Measure Four – Theta: “Bond method”

Collect full range of profiles

Performance of Mirror Optic Determined via Double Crystal diffraction

Reciprocal space map illustrates divergence between $K\alpha_1$ and $K\alpha_2$ beam directions

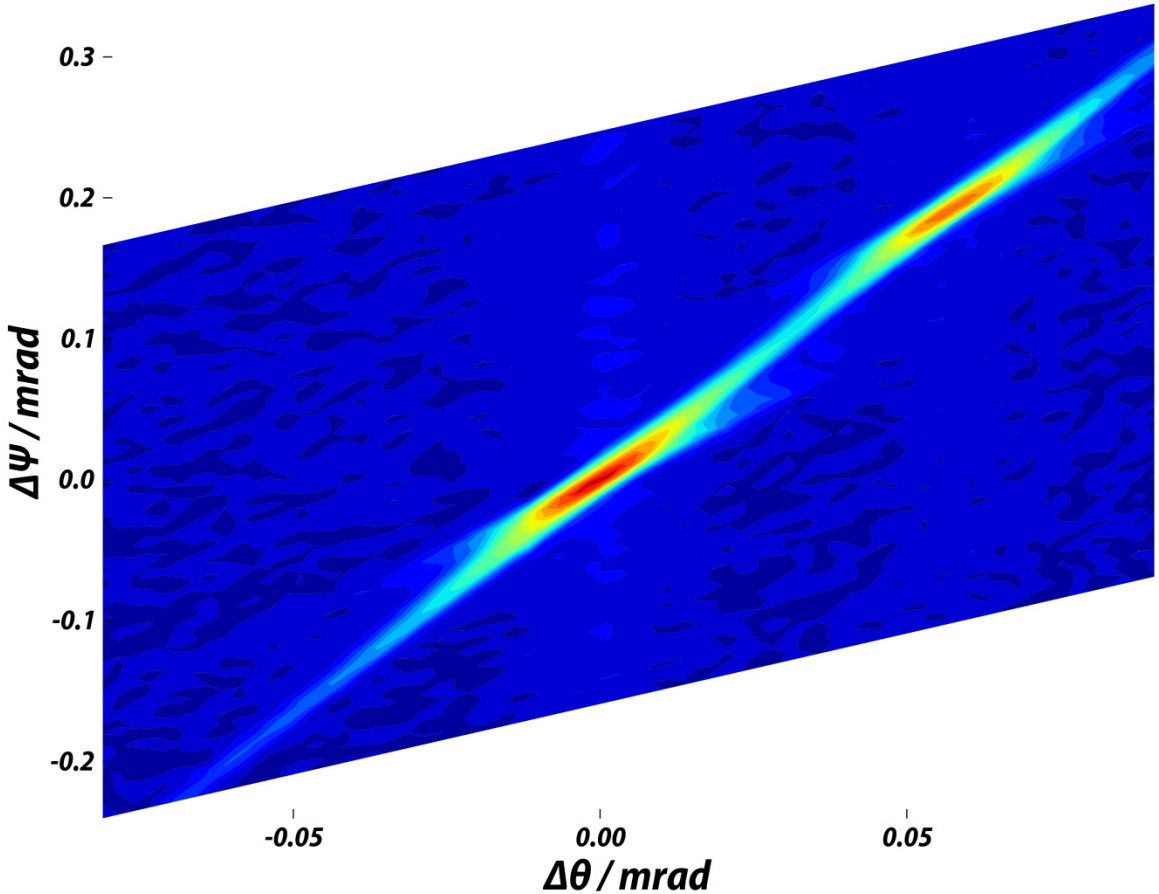

NIST – Built Divergent Beam Diffractometer (DBD)

Conventional divergent beam optics with high-performance goniometer

Second optical platform for corroboration of SI traceable measurements

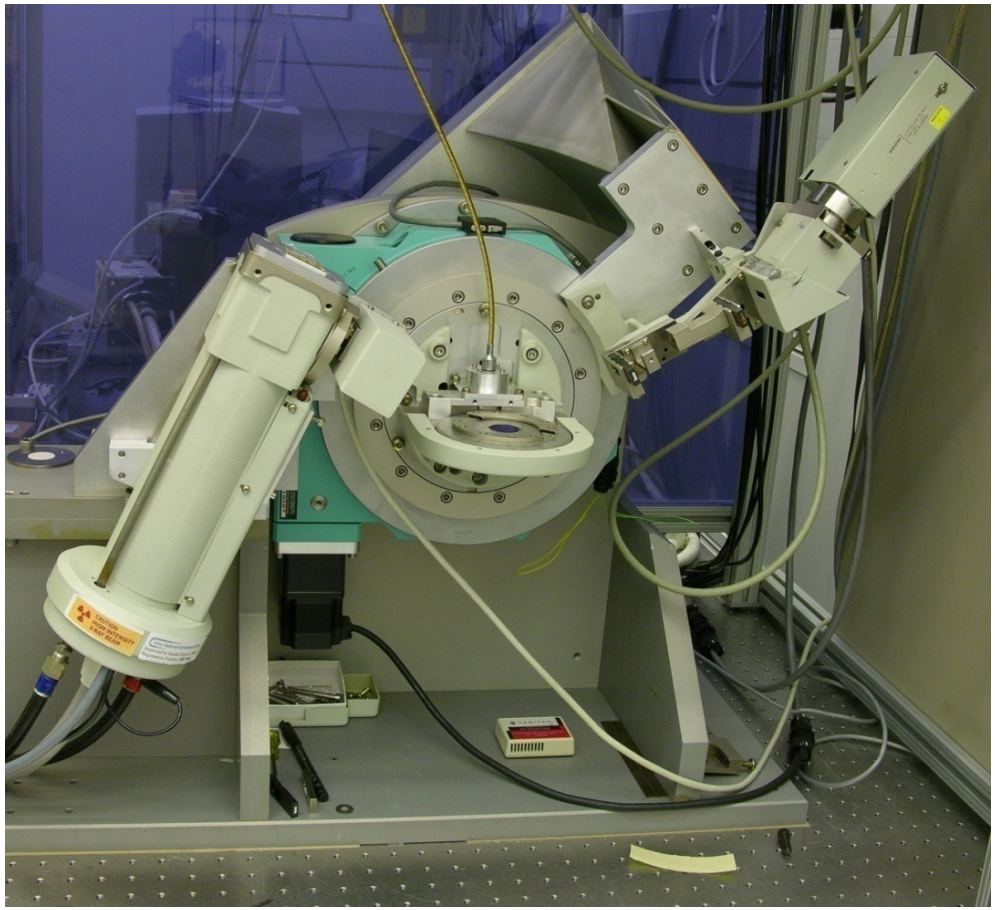

Homogeneity verification
Studies of data analysis methods
Microstructure analysis

Optics from Siemens D5000 / D500

Huber 420 rotation stages

Heidenhain RON 800 series optical encoders on primary axes

Interchangeable optics,
Incident beam monochromator

Linear PSD

Located in a temperature controlled environment ≈ ±0.1° C

Overhead diagram of DBD

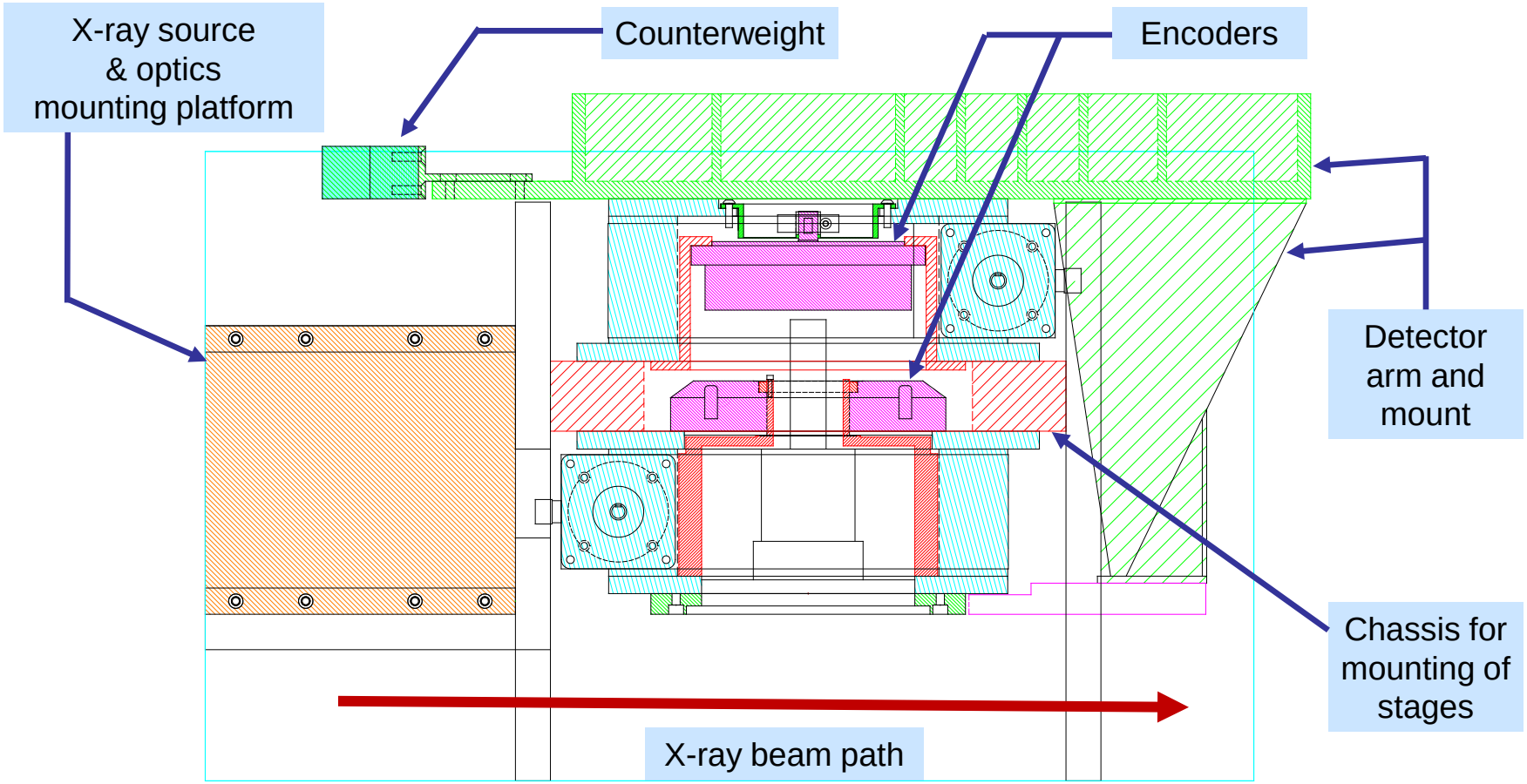

Stiff and Balanced Detector Arm

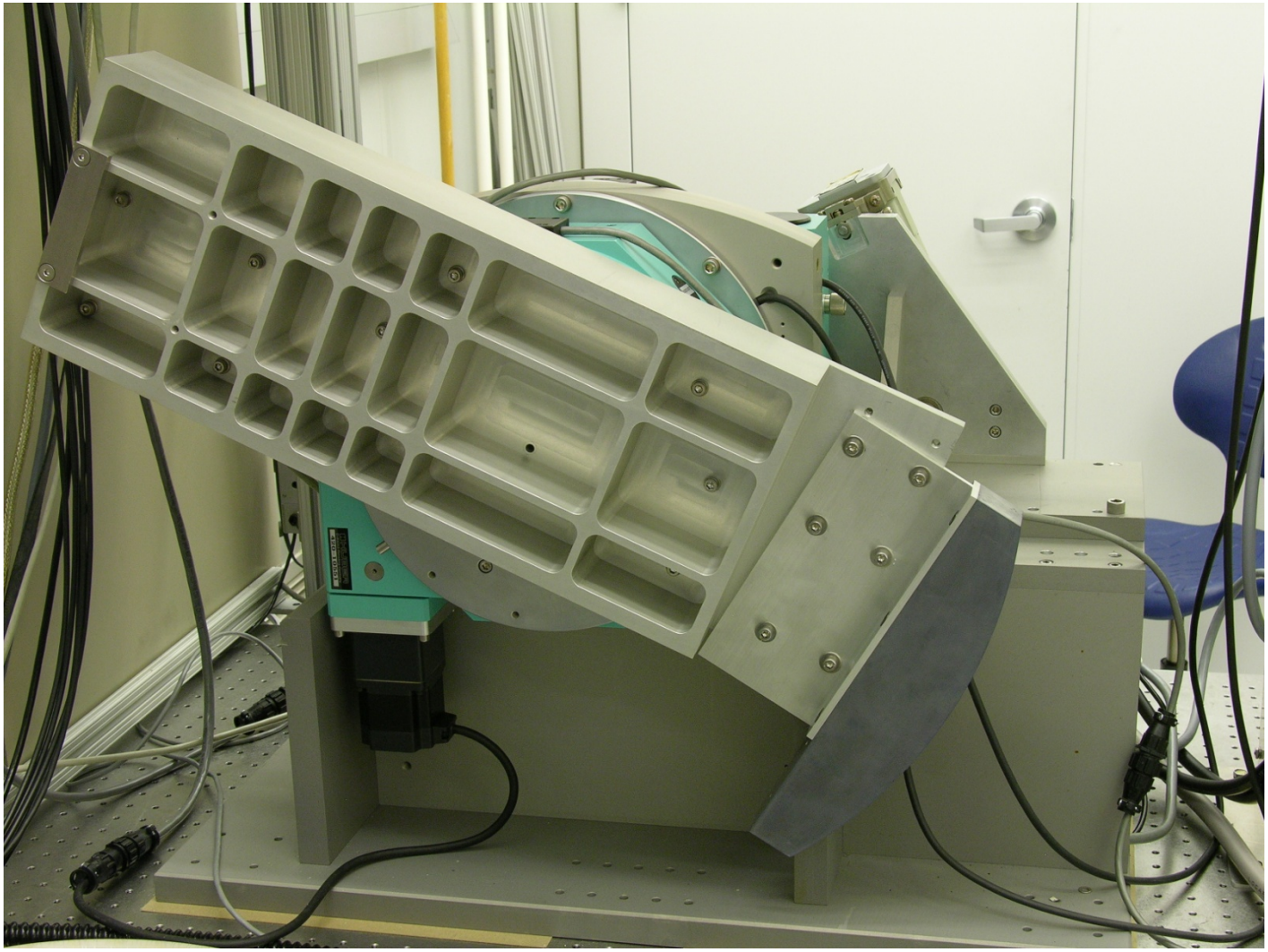

Fundamental Parameter Approach (FPA) to Analysis of Powder Diffraction Data

Cheary & Coelho (1992,1998) as implemented in TOPAS

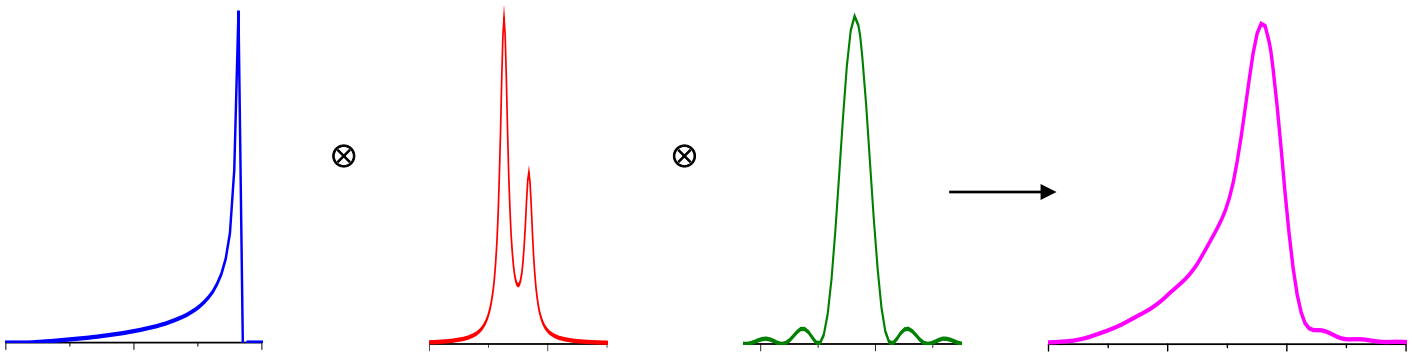

Geometric Instrument Profile ⊗ **Wavelength Profile** ⊗ **Specimen Broadening Function** → **Observed Profile**

Geometric instrument contribution characterized with a series of explicit physical models linking instrument geometry to the observed profile

Current CuKα Emission Spectrum Characterization

Hölzer, *et al*., Phys. Rev. A (1997)

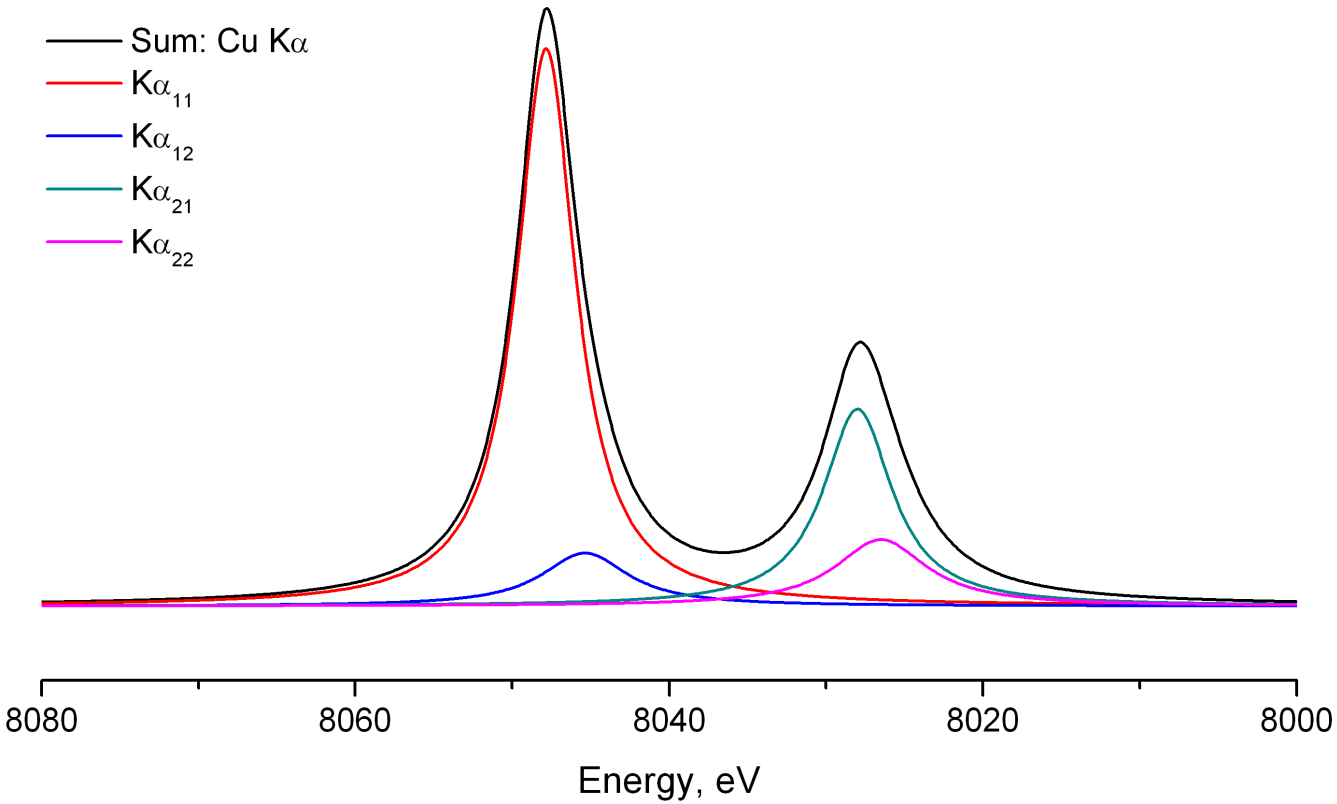

Four Lorentzian profiles used for analytical representation of the CuKα spectrum

Observation of Tube Tails & “Kα3” Satellite Lines

Proper modeling of tube tails critical for microstructure analysis

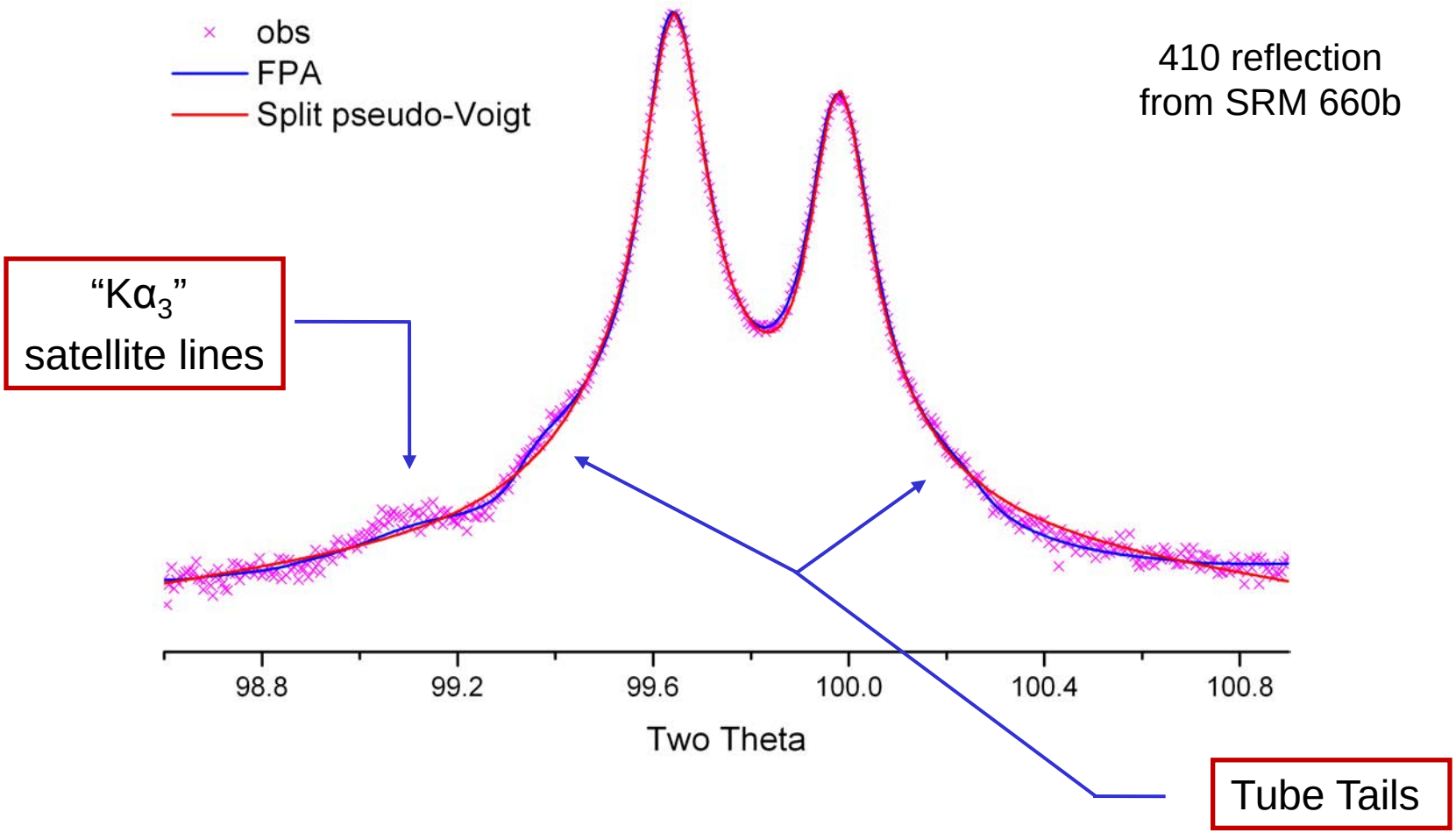

Johansson Incident Beam Monochromator (IBM)

Reflection Geometry

Anti-scatter slit located at focal point (line)

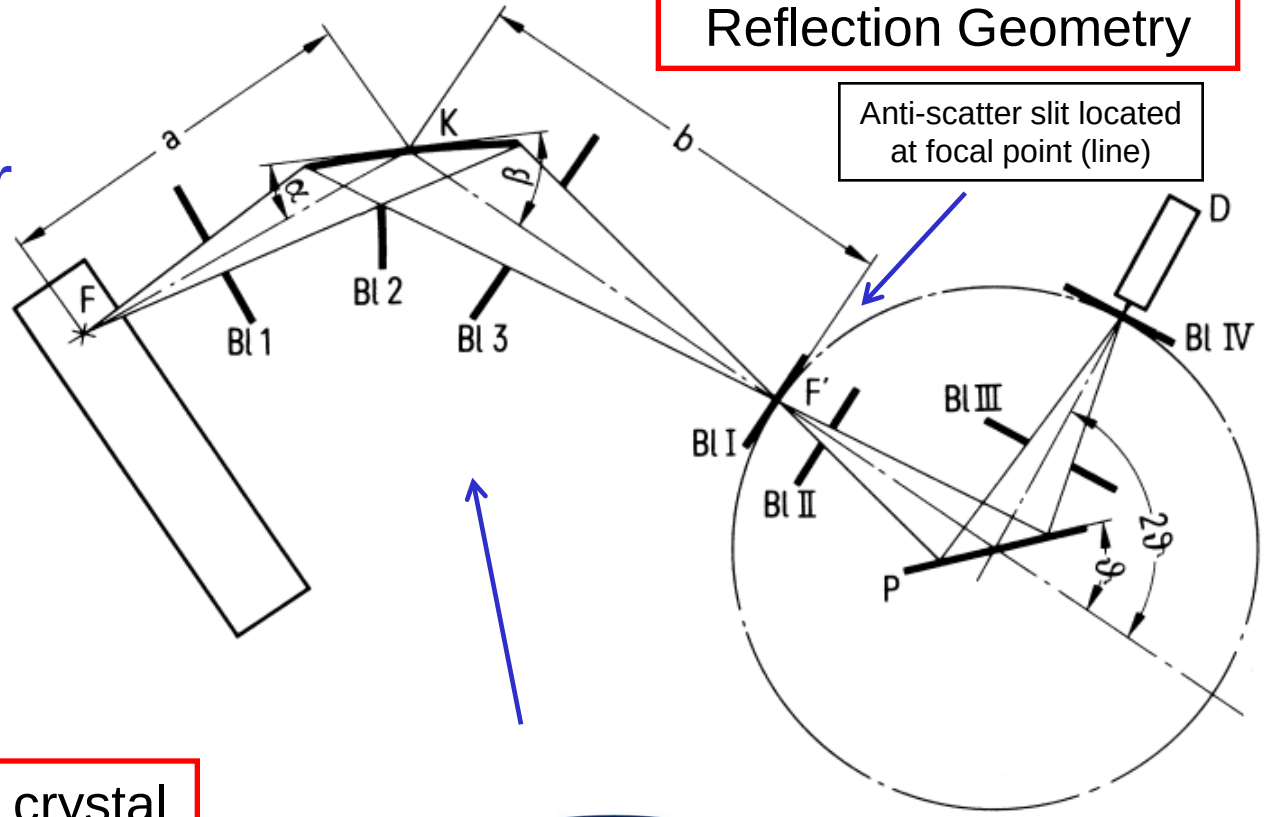

"Removes" $K\alpha_2$, $K\alpha_3$ & Tube Tails

Asymmetric Ge 111 crystal

Ground to 2R and bent to R (Rowland circle)

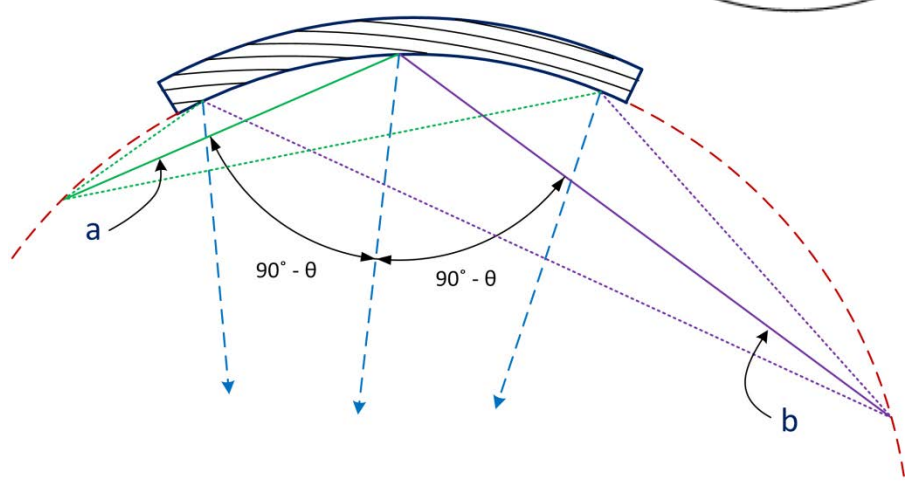

NIST – Built DBD Configured with Johansson IBM

Divergent beam optics with "monochromatic" source

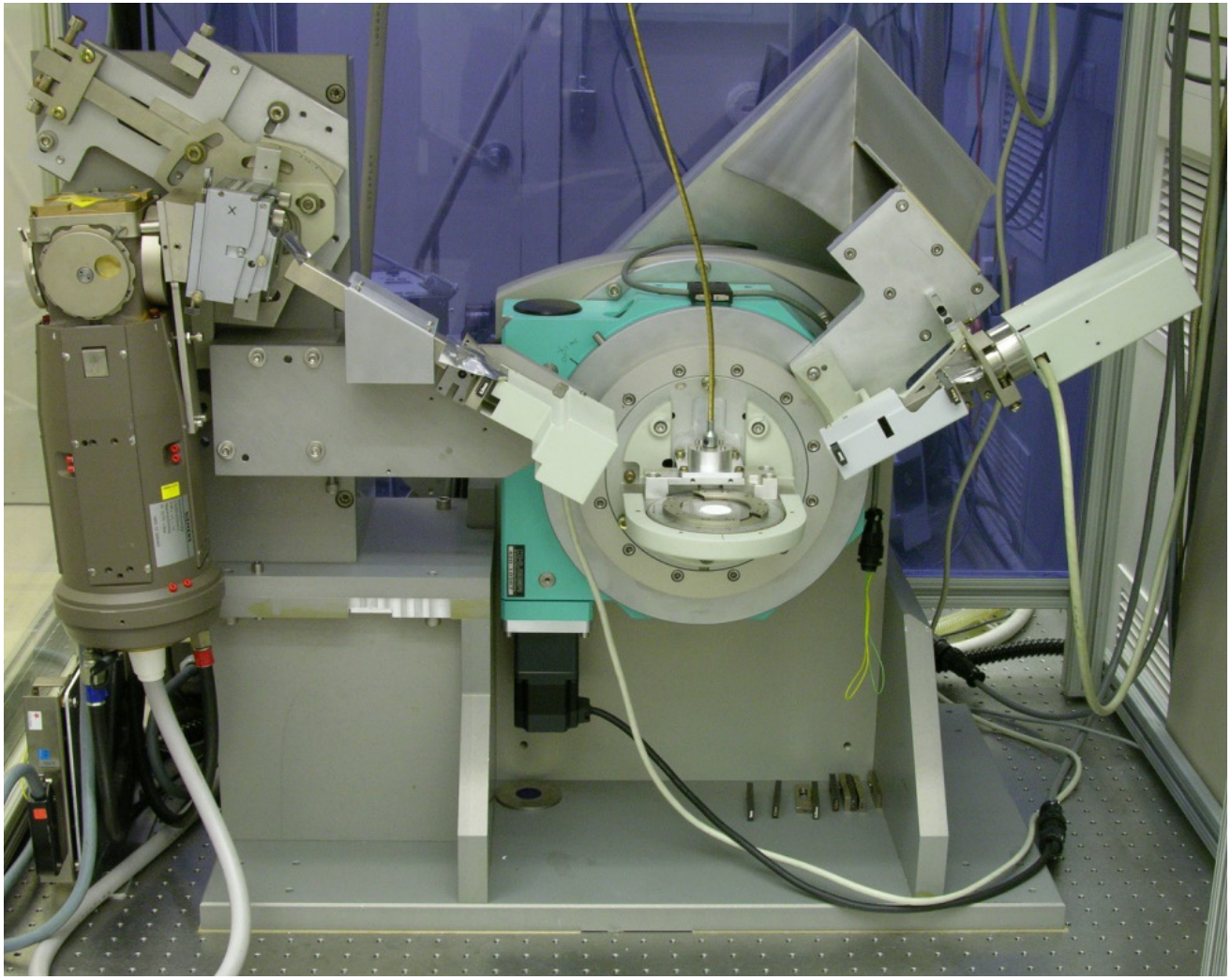

Siemens D500 tube shield with Huber 502 optic alignment:

Features fully orthogonal adjustment capability

Modern Crismatec Johansson optic

Performance of Johansson IBM

Crismatec (Saint Gobain) Johansson optic

Ge 111 crystal bent via cementing in pre-form

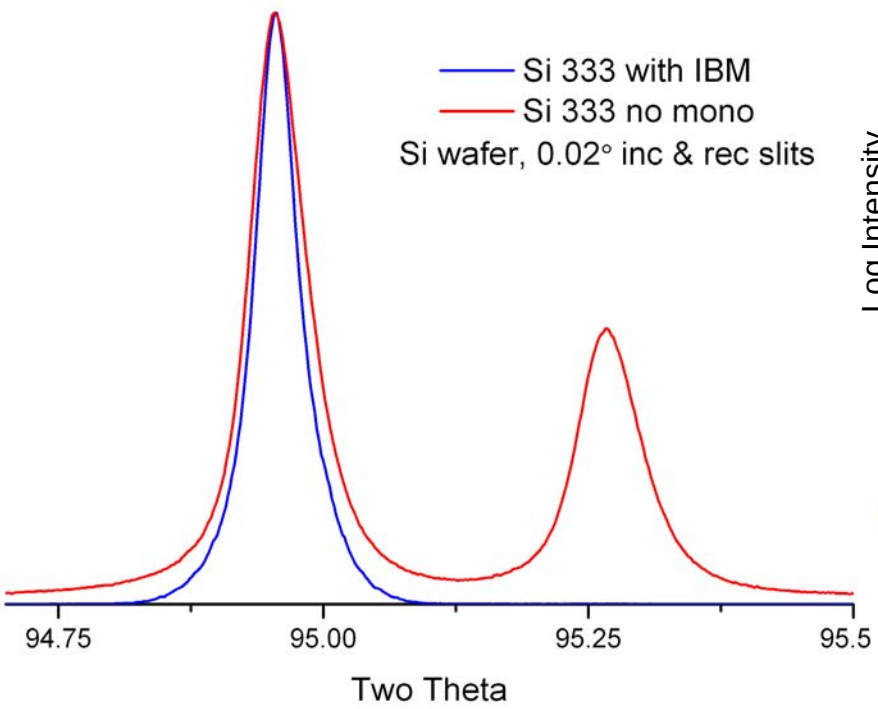

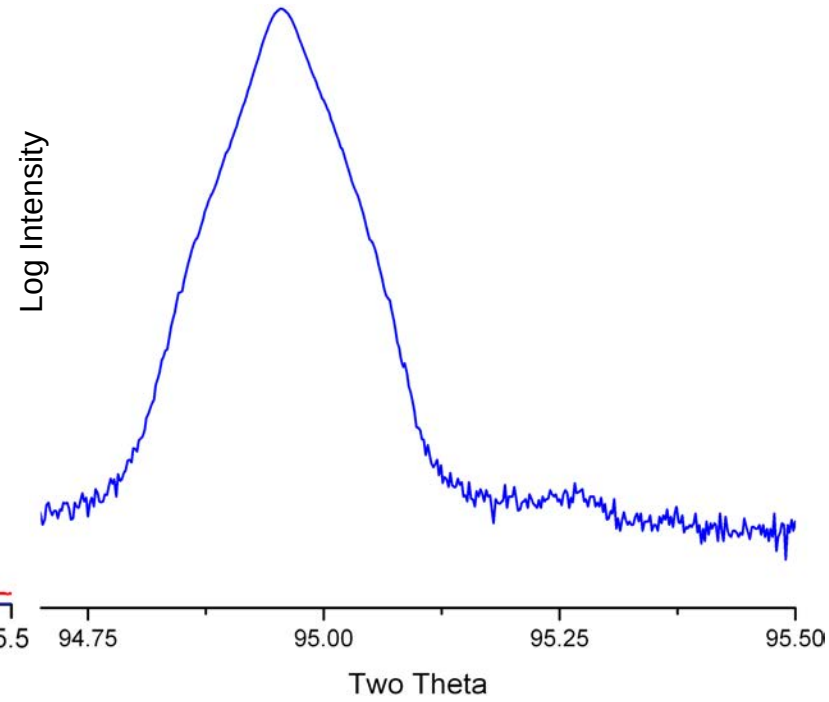

Characterization of emission spectrum for *FPA* via convolution of Gaussian profile shape functions

Fits of Split Pearson 7 PSF to IBM data

Excellent fit quality to IBM data using analytical PSF

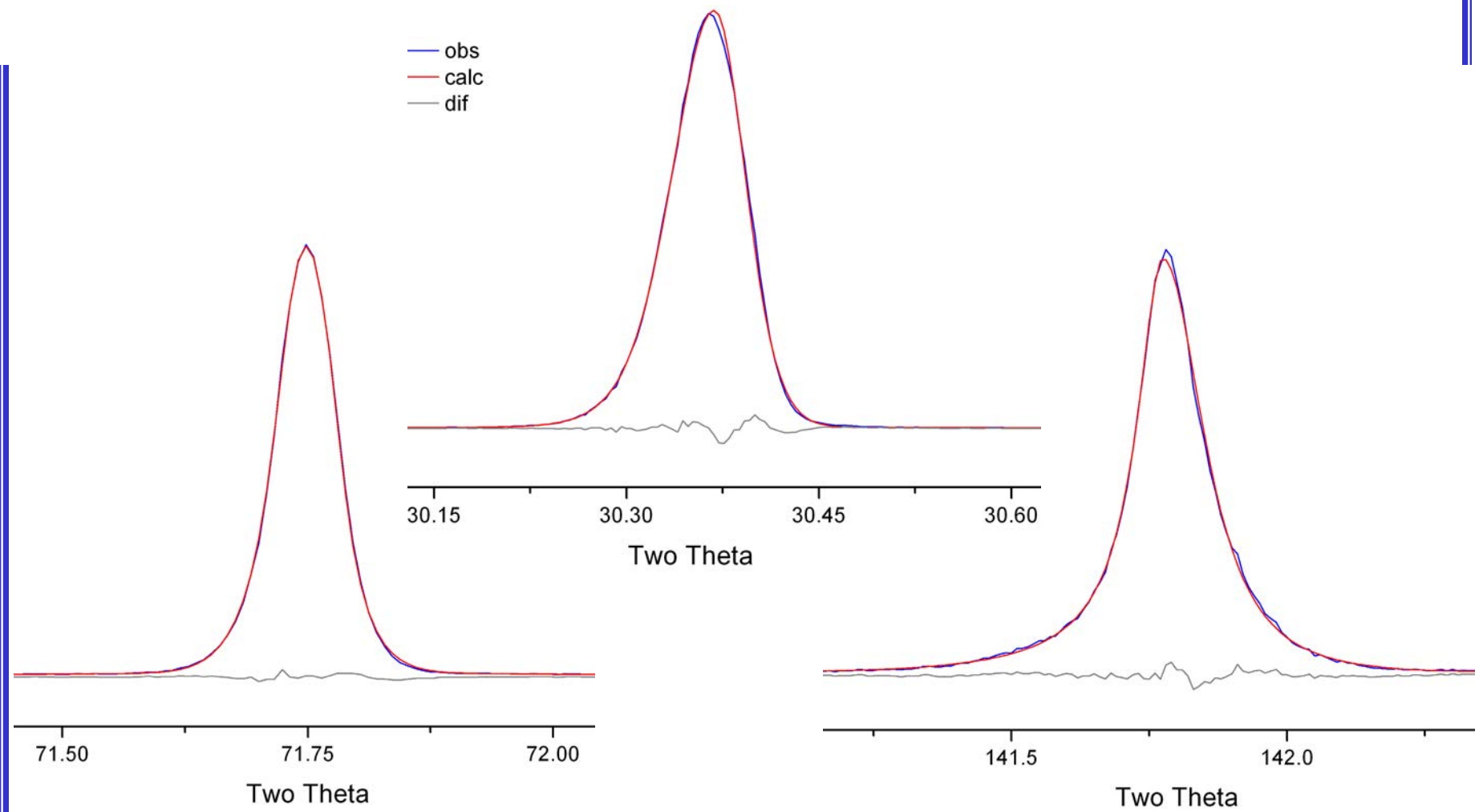

FWHM data from SRMs 640d, 660b and 1976b

FWHM values follow trends consistent with expectations as per contributions from Geometric and Wavelength Profiles

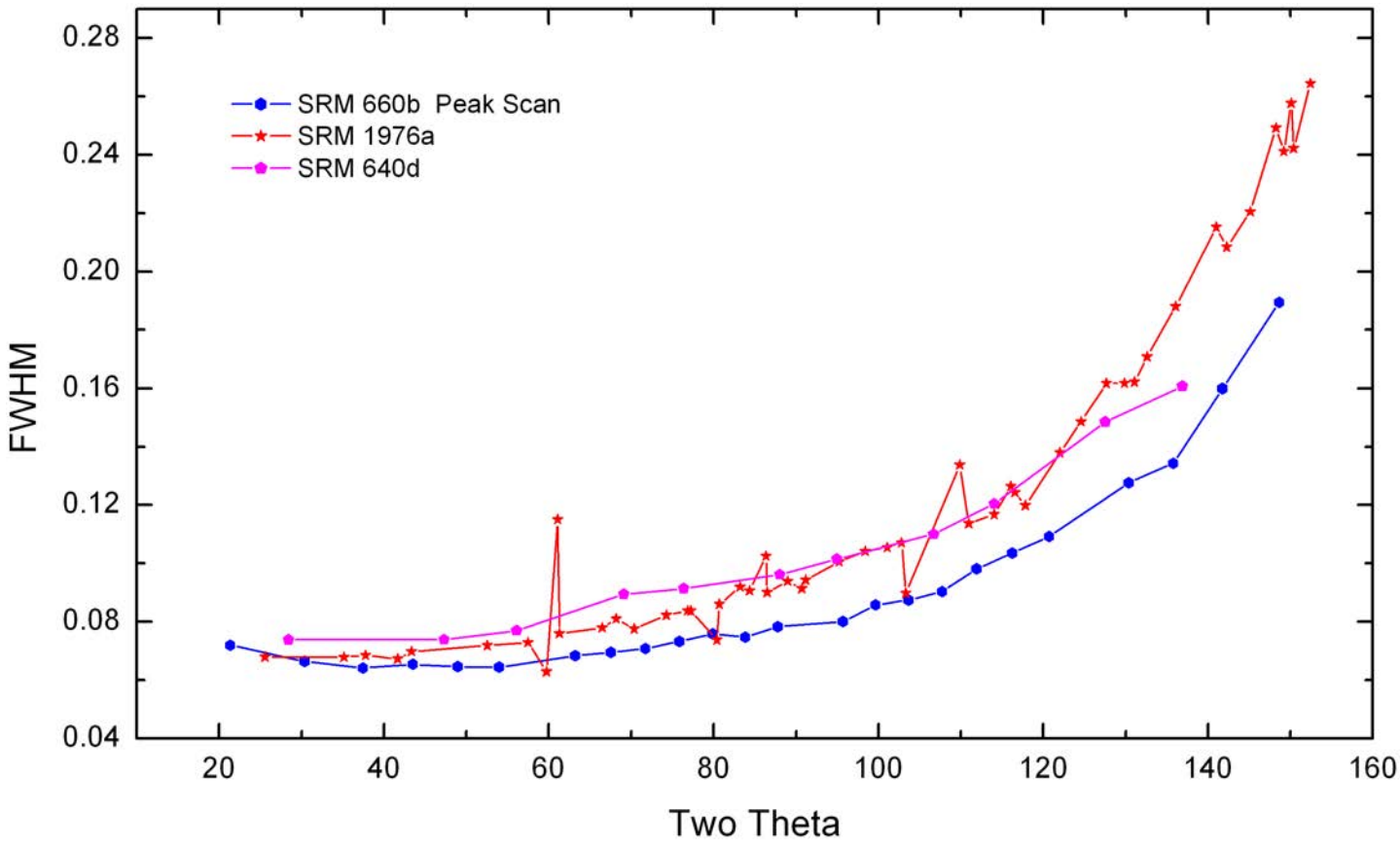

Parameters Affecting Geometric Profile

Divergent beam laboratory X-ray powder diffractometer

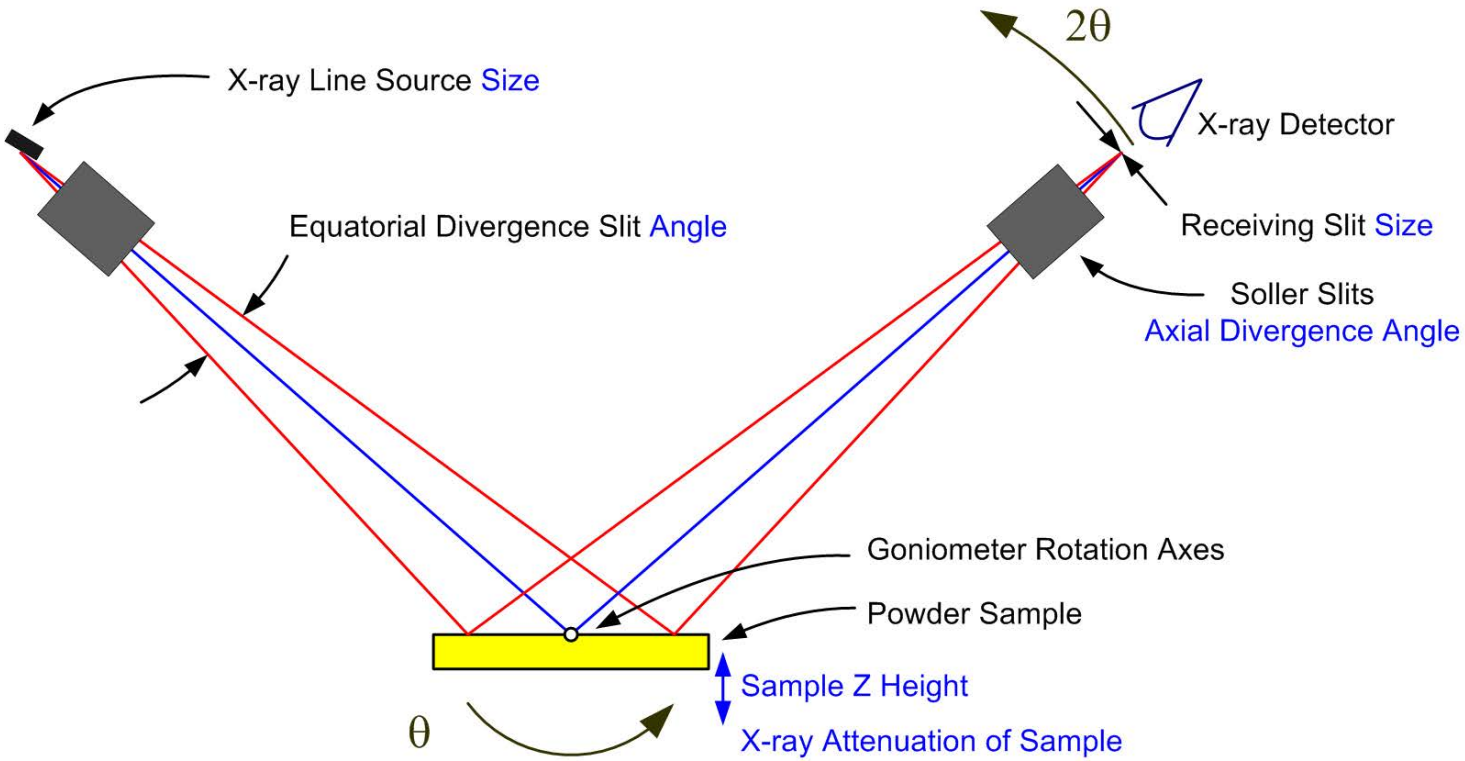

Aberrations Contributing to Geometric Component

May affect both profile shape and position

Aberration	Controlling parameters	Impact
X-ray Source Width (w_x)	Angle subtended by source: $\frac{w_x}{R}$	Symmetric broadening
Receiving Slit Width (w_r)	Angle subtended by slit: $\frac{w_r}{R}$	Symmetric broadening
Flat Specimen Error / Equatorial Divergence	Angle of divergence slit: α	Asymmetric broadening to low 2θ, with decreasing 2θ
Axial Divergence Case 1: No Soller slits Case 2: Soller slits define divergence angle	Axial lengths of the x-ray source (L_x) sample (L_s) & receiving slit (L_r) relative to goniometer radius (R) Acceptance angles Δ_I and Δ_D of the incident and diffracted beam Soller slits	Below ≈ 110°: Asymmetric broadening to low 2θ, with decreasing 2θ Else to high 2θ, with increasing 2θ
Specimen transparency	Penetration factor relative to diffractometer radius $\frac{1}{\mu R}$	Asymmetric broadening to low 2θ, with Sin(θ)
Specimen Displacement Z height	Displacement of specimen surface from goniometer rotation axes	Displacement of profiles with 1/Cos(θ)

Diagram of an Aligned X-ray Diffractometer

Functionality of FPA dependent on proper alignment

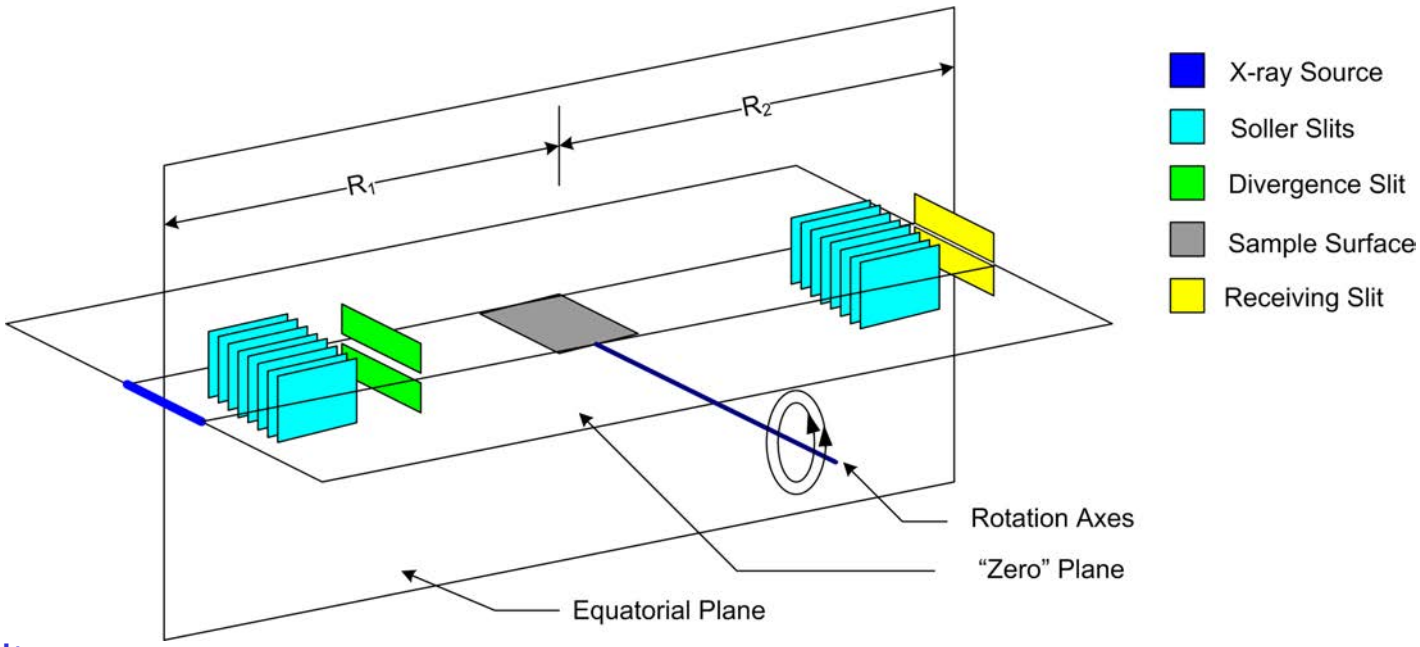

Requisite on:

1) Source-to-sample distance equals sample-to-receiving slit distance ($R_1 = R_2$)
2) X-ray line source, sample, and receiving slit centered in plane of diffraction
3) Goniometer rotation axes are co-axial

→ X-rays off

4) X-ray line source, sample surface, receiving slit, and goniometer rotation axes are co-planar, in the "zero" plane, at zero angle of theta and two-theta
5) Incident beam is centered on both equatorial and "zero" planes

→ X-rays on

Data Analysis Strategy

Determine extent and nature of flaws in FPA model

Compare refined lattice parameters from FPA Rietveld analysis with those from FPA "Profile" analysis

Always refine parameters that are indeterminate

Sometimes refine parameters that are known or essentially invariant between standards and unknowns

Never refine parameters that well known and correlate with unknowns

Always Refine:

Axial divergence value
[inc and rec values constrained to identity]
Z height
Specimen transparency
Position & intensity of $K\alpha_2$ lines
Structural model(s)
Microstructure model(s)

Sometimes Refine:

Breadth of $K\alpha_1$ and $K\alpha_2$ lines
Inc and rec slit values
"Tube Tail" parameters
"$K\alpha_3$" line intensity

Never Refine:

Zero angles

Fundamental Parameters Analysis of SRM 660b

FPA “profile” analyses: Profile positions (lattice parameters) free to refine, FPA shape parameters constrained

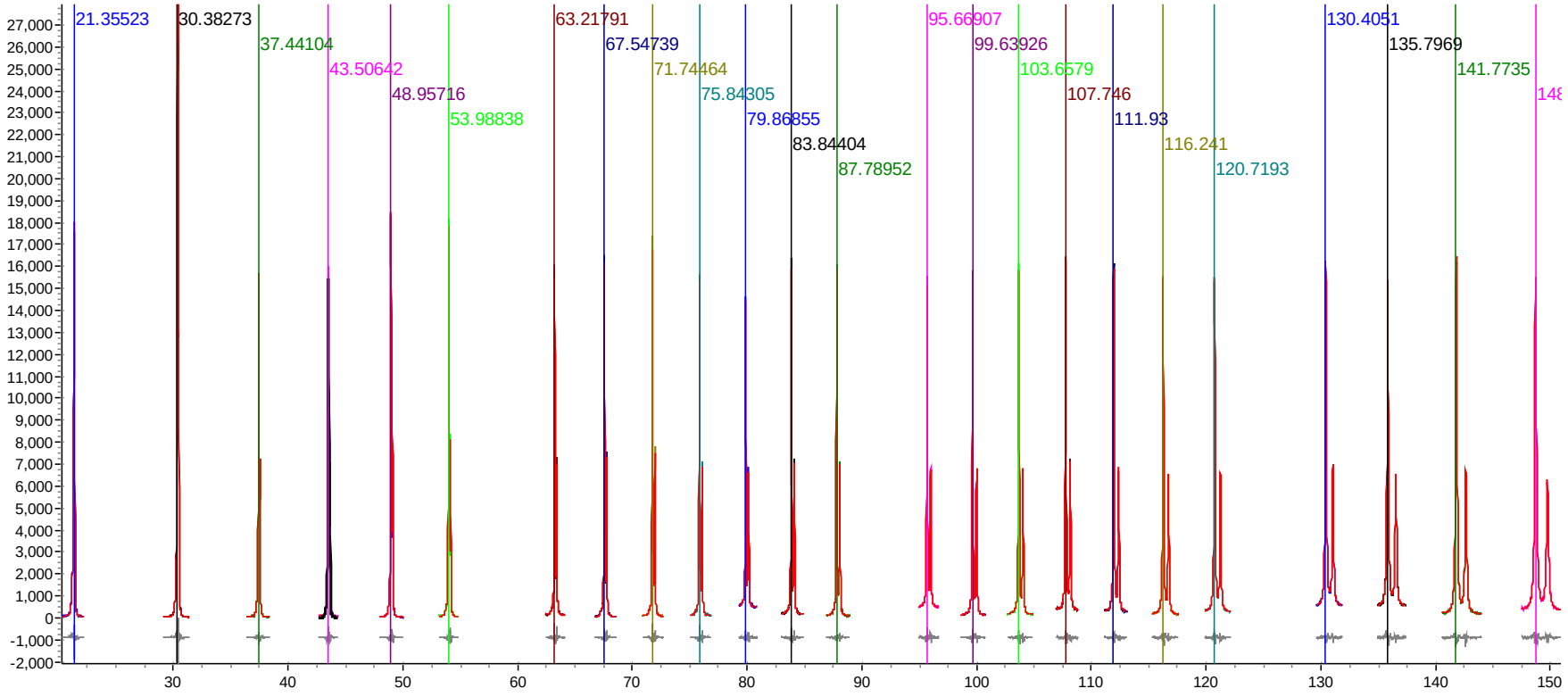

Plausible parameters realized throughout *

Impact of Graphite Post Monochromator on Breadth of CuKα Emission Spectrum

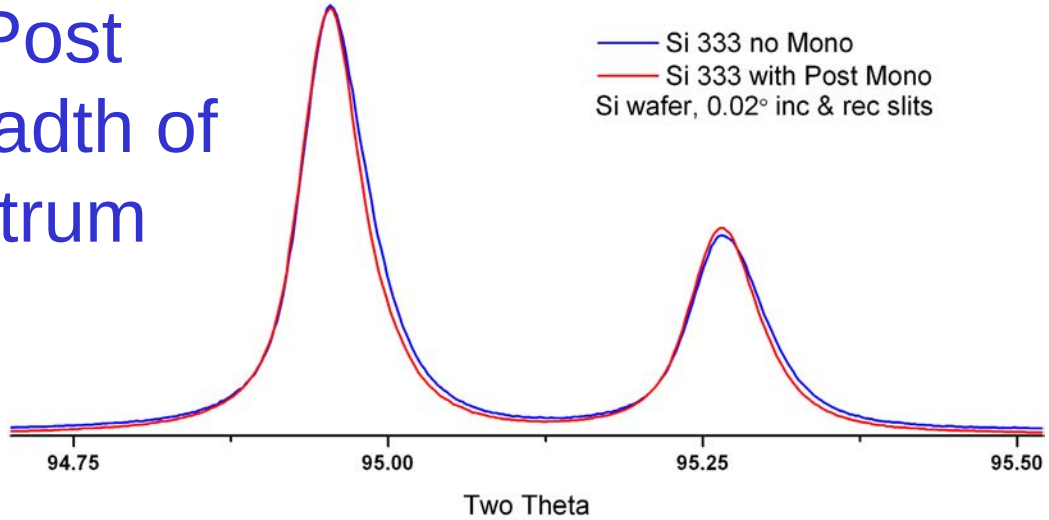

20% Reduction in breadth

Shift of 0.01˚

```
.
for xdds {.
   LP_Factor( 26.6).
   lam.
      ymin_on_ymax  0.0001.
      la sat  0.0080`_0.000213173601 lo  1.534753 lh  3.6854.
      la  0.5711 lo  1.540591 lh lhll  0.3314`_0.00240437679.
      la  0.0781 lo  1.541064 lh =lhll 1.47; :  0.4871`_0.00353443388.
      la la2l  0.2565`_0.000255806605 lo l2l  1.544386`_4.98191335e-007 lh lh2l  0.4022`_0.00261264019.
      la =la2l .36; :  0.0923`_9.20903777e-005 lo =l2l+.0003; :  1.544686`_4.98191335e-007 lh =lh2l 1.4; :  0.5631`_0.00365769627.
   Specimen_Displacement(-0.00192).
   x_calculation_step = Yobs_dx_at(Xo); convolution_step 4.
   Rp 217.5.
   Rs 217.5.
   Slit_Width( 0.2).
   Divergence( 0.8).
   axial_conv .
      filament_length  12.
      sample_length  15.
      receiving_slit_length  15.
      primary_soller_angle ssl  5.3752411`_0.00751067001.
      secondary_soller_angle ssl  5.3752411`_0.00751067001.
      axial_n_beta  30.
   Tube_Tails(, 0.04,ttl, -1.06559`_0.00431,tt2, 1.18058`_0.00390,ttf, 0.00102`_0.00025).
   Absorption(672.35363).
```

Portion of Topas .inp file illustrating refinement of profile breadths

Shape of $K\alpha_1$ and $K\alpha_2$ lines constrained to that defined by Hölzer

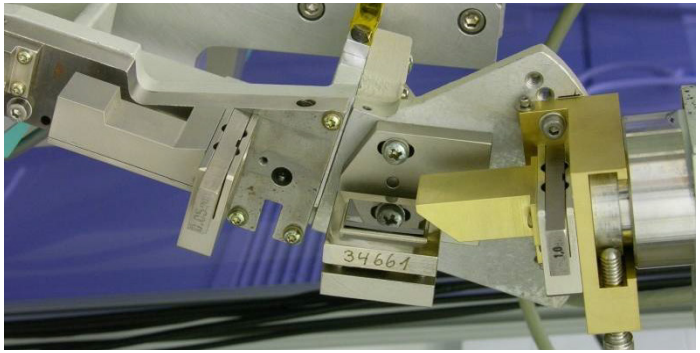

Comparison of Lattice Parameter Data from FPA Rietveld vs. Profile

No Complaints; However, trends are indicated

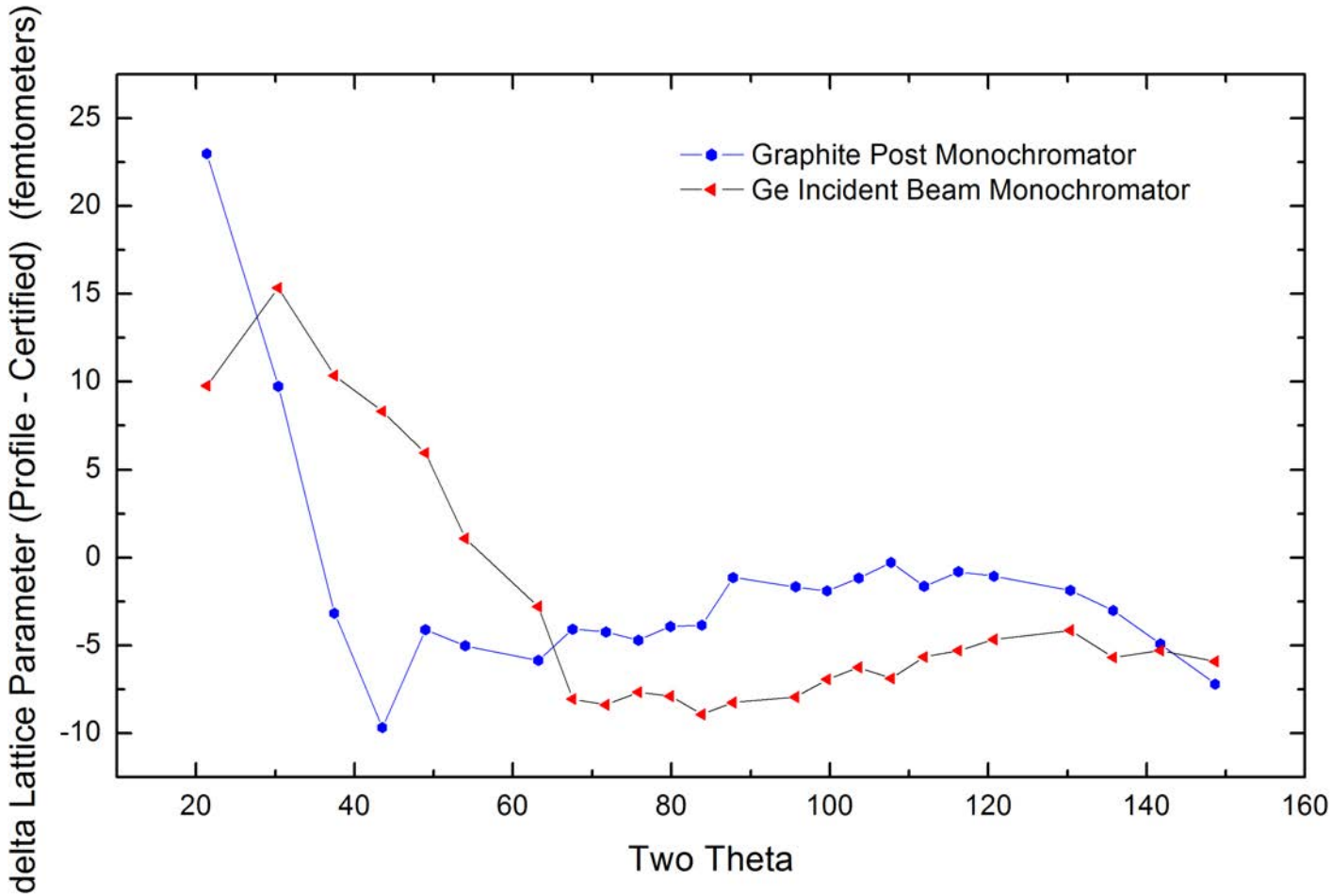

Comparison of Lattice Parameter Data from FPA Rietveld vs. Profile: Certification of SRM 660b

Type A (statistical) vs. Type B (systematic) error bounds

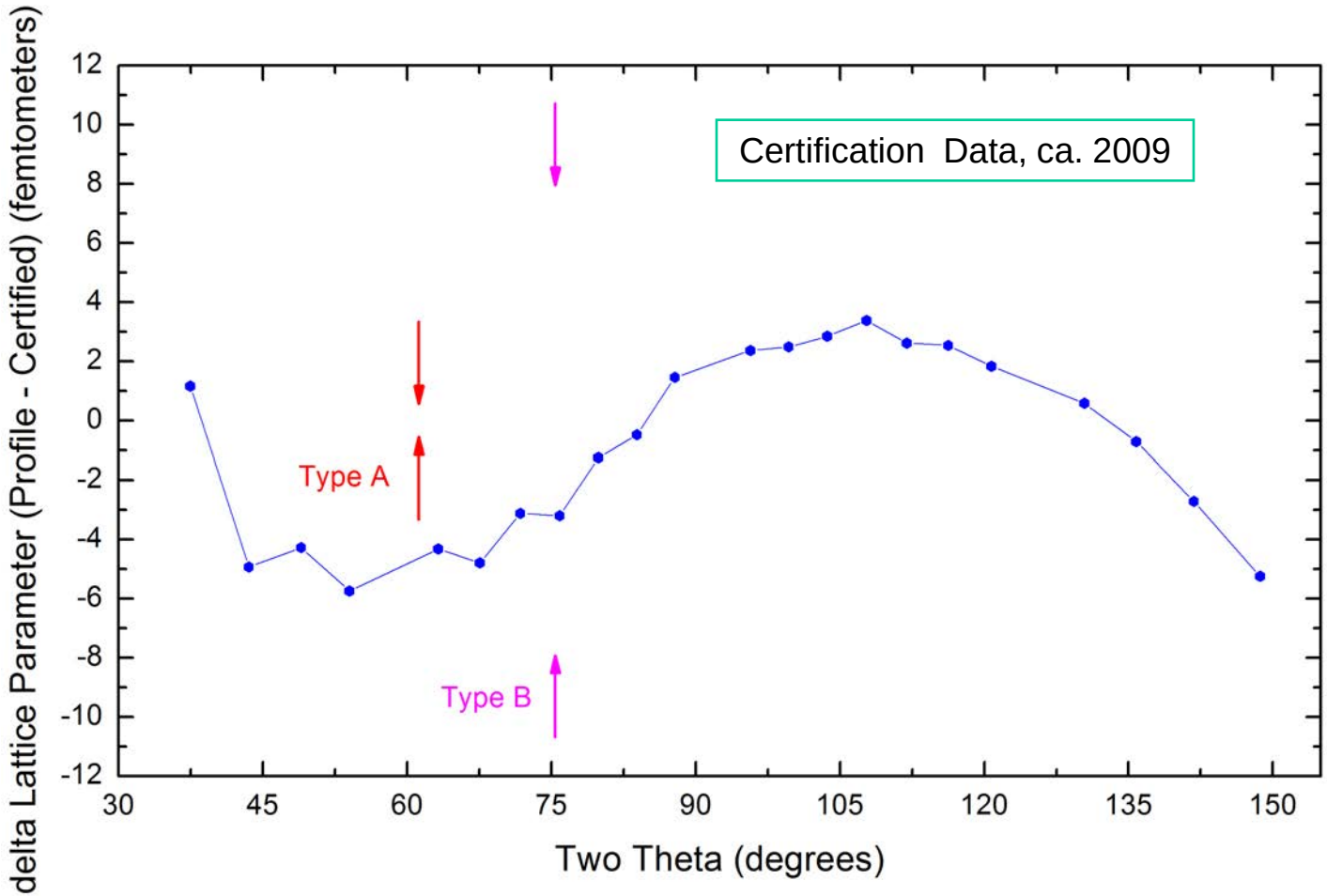

Finite Element Analysis of Change in Torque Moment with Rotation of Two-Theta Arm

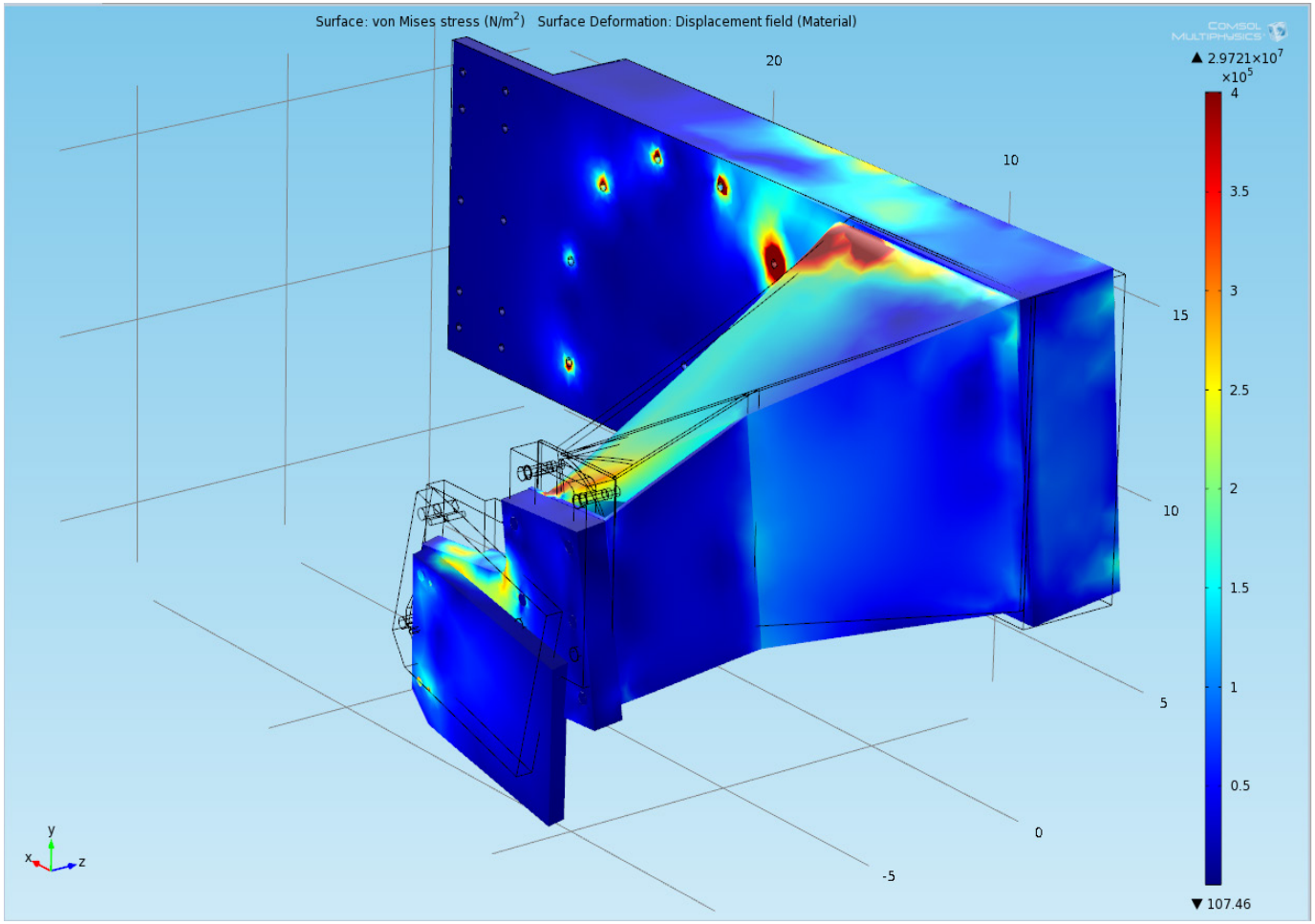

Quantitative Rietveld Analysis, QRA

Diffraction experiment assesses crystalline component only

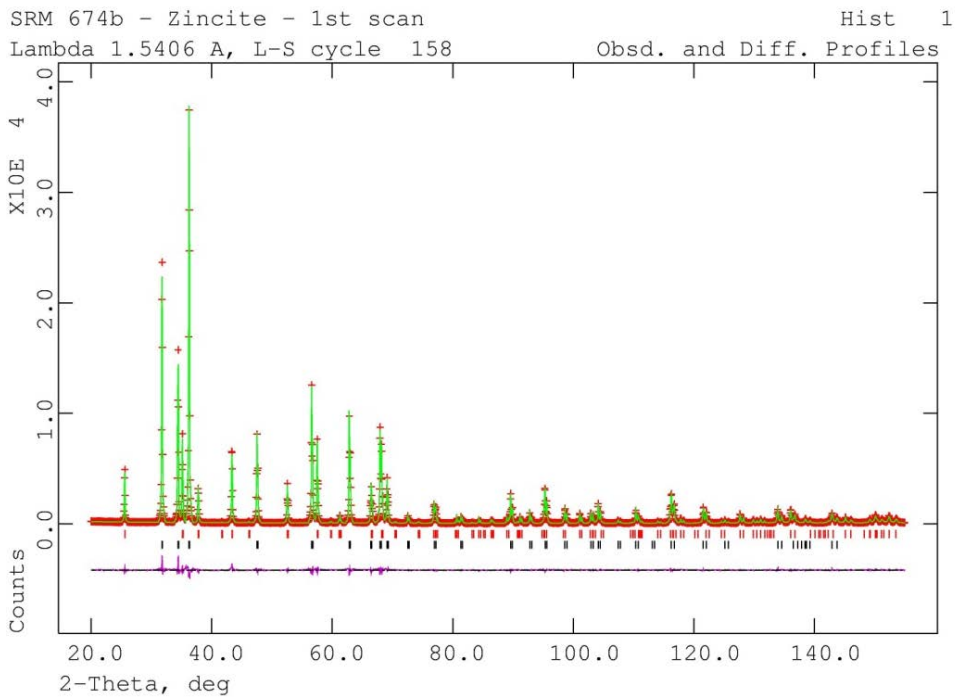

Quantification via GSAS:

$$\frac{X_\alpha}{\sum_{k=1}^{n} X_k} = \frac{S_\alpha Z_\alpha w_\alpha}{\sum_{k=1}^{n} S_k Z_k w_k}$$

X_α is the mass fraction of phase α
S_k are the scale factors
w_k are the molecular weights
Z_k are the number of formula weights per unit cell

$$\sum_{k=1}^{n} X_k = 1$$

Suitable Standard: $X_s = X_{s(xtal)} + X_{s(amor)}$ Yields:

$$\frac{X_{s(xtal)}}{\sum X_{u(xtal)} + X_{s(xtal)}} = \frac{S_s Z_s w_s}{\sum S_k Z_k w_k}$$

$$\sum X_{u(xtal)} + X_{u(amor)} = 1 - X_s$$

Amorphous Component of Finely Divided Crystalline Solids

One crystallographic unit of thickness on 0.2 μm particles: 0.75% amorphous content

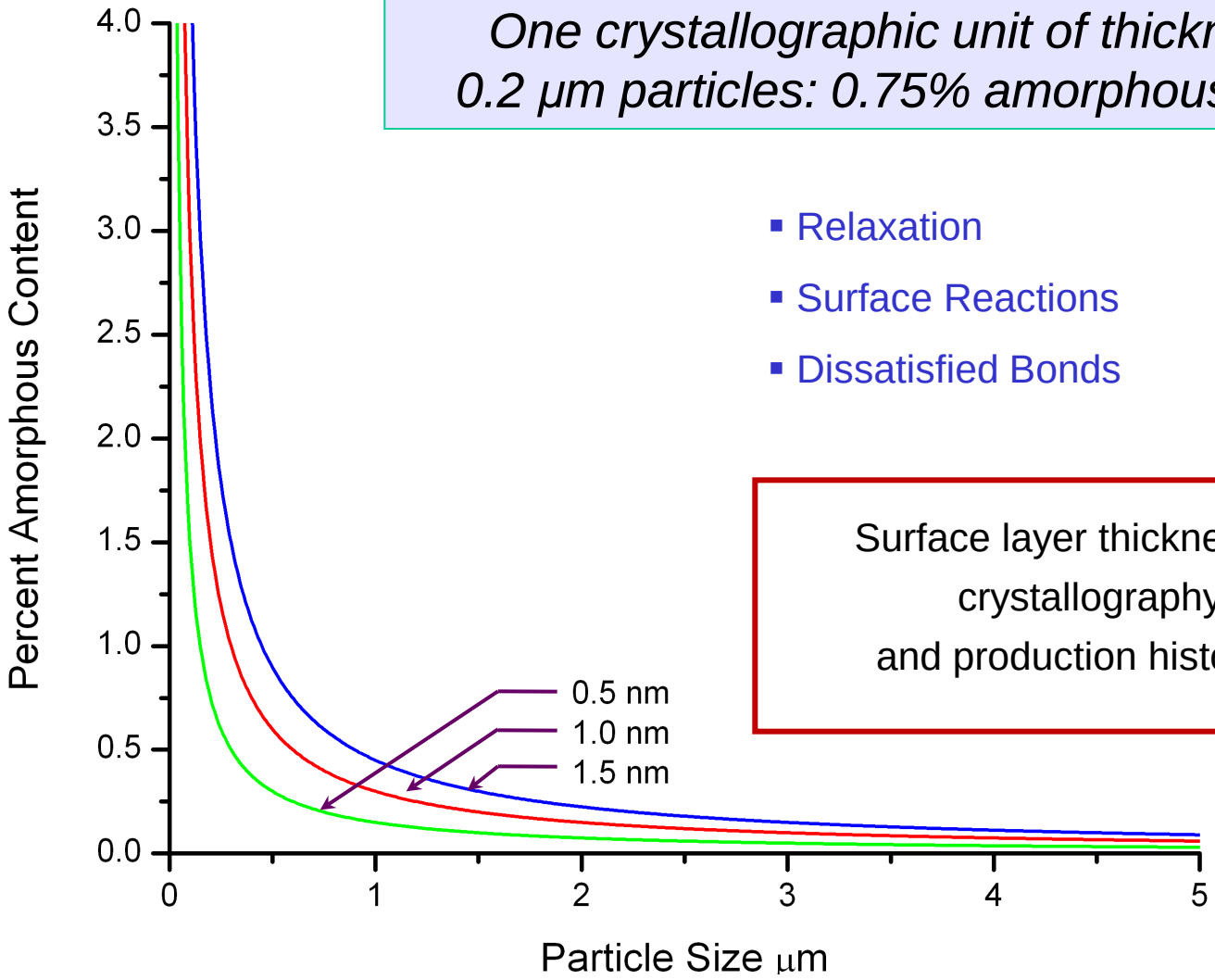

- Relaxation
- Surface Reactions
- Dissatisfied Bonds

Surface layer thickness determined by crystallography, chemistry and production history of the powder

Selection of an Alumina Powder for use as an Internal Intensity (Quantitative Analysis) Standard

I/I_c Proposed by Visser and deWolff (1964)

Property included in ICDD database; hence SRM 676(x)

Desired characteristics of SRM feedstock

- strong lines over a wide d-space range
- stability
- inertness
- equi-axial (non-orienting) particles
- particle size in the one micrometer range: microabsorption (Brindley, 1945)
- small diffracting domains: primary extinction (Zachariasen, 1945)

Selection of an Alumina Powder for use as an Internal Intensity Standard

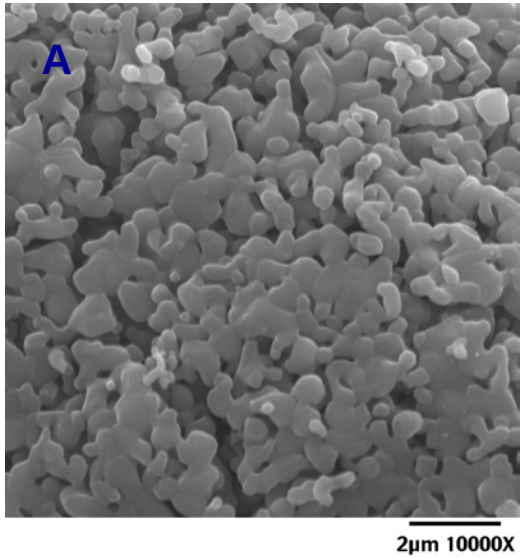

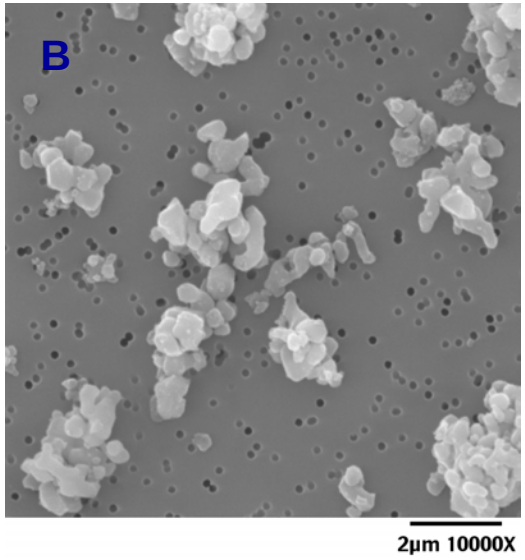

Commercial Alumina Production

95% via Bayer process:

Low T: Transition alumina impurities "Active Alumina"

High T: Platelike coarse grains "Tabula Alumina"

Material not well suited for use as a standard

Dynys and Halloran (1982) :

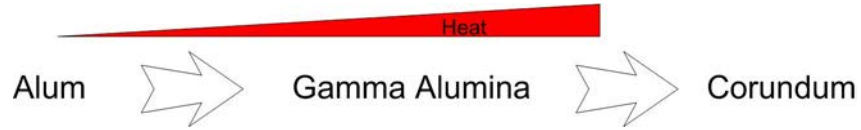

Low T: Phase pure alumina w/ "sponge" microstructure **A**

With comminution: Equiaxial fine grains **B**

Material quite well suited for use as a standard

SRM 676a Feedstock Consists of Baikalox* CR1

Alum process *Calcined to 1400°C* *Jet milled*

Particle size via laser scattering

%<	µm
10	0.58
50	1.28
90	2.82

*Baikowski Chimie, France

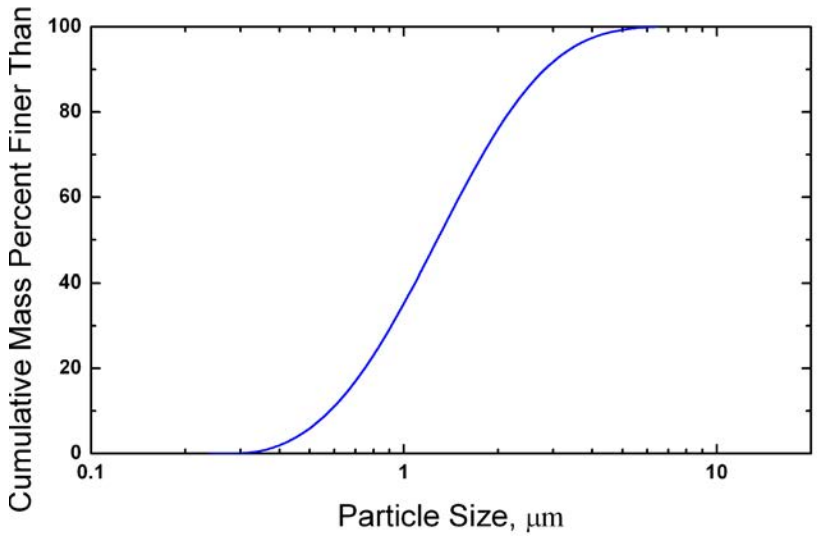

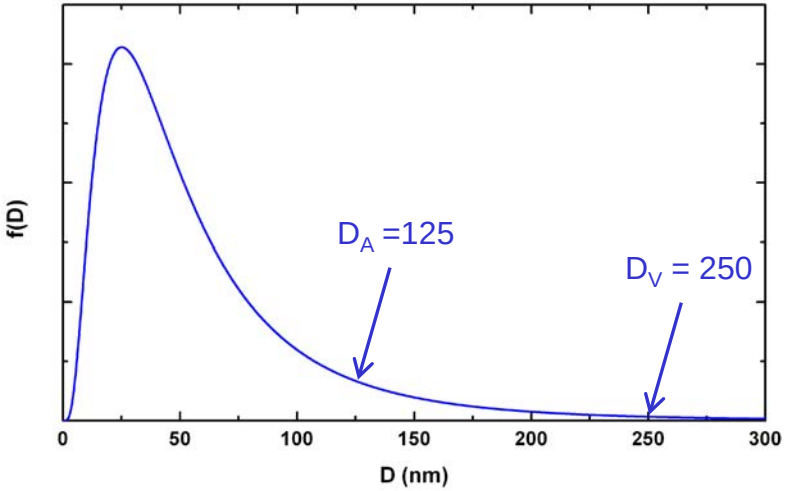

Crystallite size via profile broadening

Data from 11 BM, APS, SRMs 660a & 676a

Analysis via TOPAS

Distribution via Krill & Birringer (1998)
Popa & Balzar (2002)

Implementation via P. Whitfield

Determination of Amorphous Fraction I

Diffraction experiment: crystalline fraction only
Weighing operation: all constituents

Experimental Design

No possibility for phase pure reference material
- Vary impurity level in systematic manner
  - Engineer microstructure so as to ensure said variation

Single crystal reference material; as per silicon of SRM 640c
- Amorphous material restricted to surface (oxide) layer
  - Surface layer of uniform thickness, invariant with respect to particle size
    - Variation of particle size / surface area in series of single crystal powders
      - Diffraction experiments on series of two phase mixtures, reference vs. test
        - Extrapolate diffraction results to reference phase of “zero” amorphous content
          - Compare diffraction result from test phase to mass fraction of weighing operation

Determination of Amorphous Fraction II

Execution

Comminute silicon to broad size distribution & anneal

Fractionate into five lots from 5 - 25 micrometers

Measure surface area & particle size

Prepare 4 X 50-50 mixtures, plus SRM 640c

Accurate diffraction experiments

Multiple diffraction methods/facilities

Address extinction effects within QRA

Plot refined mass fraction silicon vs. surface area

Extrapolate mass fraction trend to a silicon with “zero” surface area

Contrast with 50-50 mass fraction: phase purity of SRM 676a

Slope yields oxide layer thickness on silicon

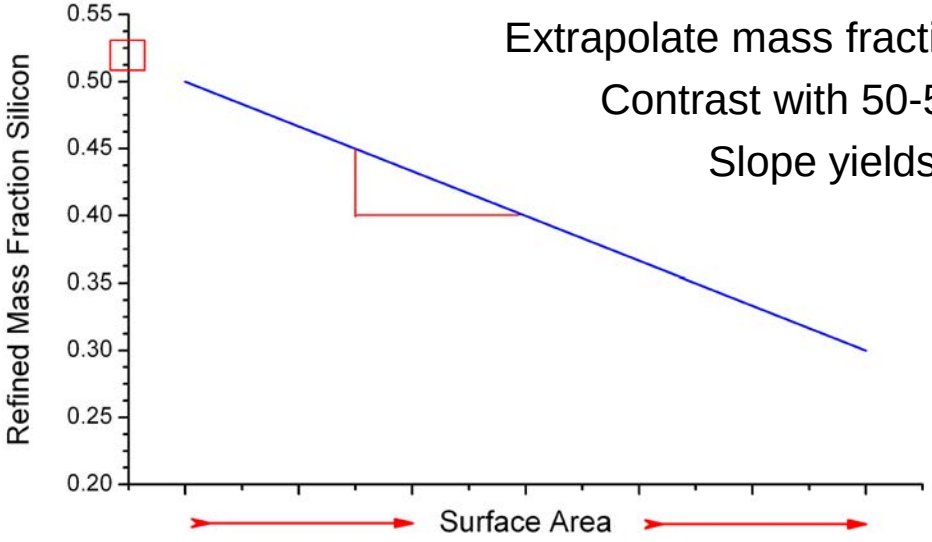

Microstructure Data on the Five/Six Lots of Silicon

Sieve Fraction	SRM 640c	< 5 μm	5 < 10 μm	10 < 15 μm	15 < 20 μm	20 < 25 μm
Particle Size, μm	4.44	5.28	9.81	14.47	19.24	23.98
Surface Area, m^2/g	1.40	1.50	0.70	0.41	0.31	0.27

Annealed in gettered argon at 1000°C for 2 h, van Berkum, et al. (1995)

Electro-deposited sieves, 5,10,15,20 & 25 μm

Sieved in anhydrous isopropyl alcohol, wash w/ dilute nitric acid

Size distribution via laser scattering

Surface area via BET adsorption, krypton

Image of Equipment Used for Annealing of Silicon in ultra-low P_{O_2} Ar

Silicon oxide surface layer reduced to elemental silicon

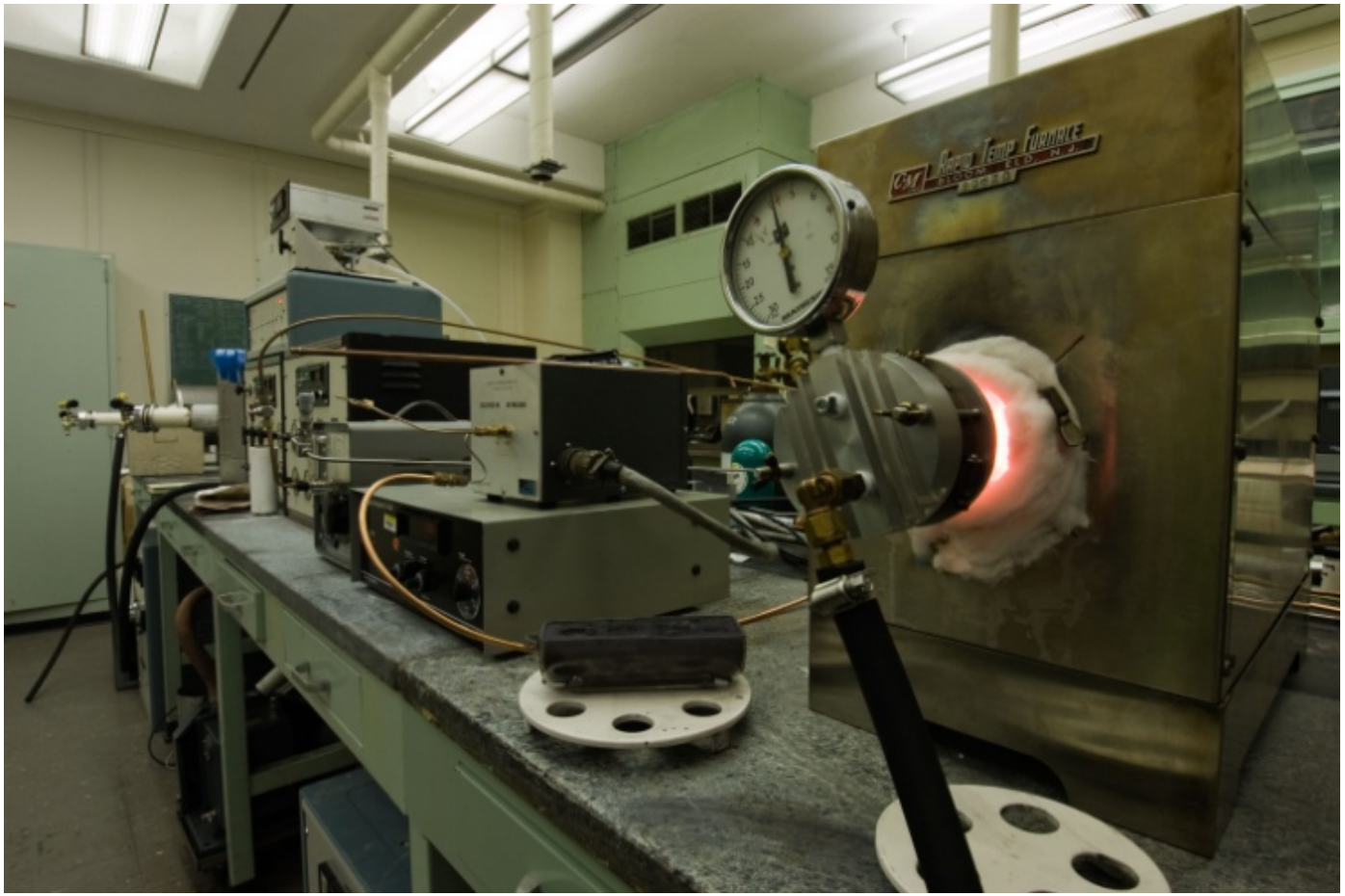

Primary Extinction

Dynamical scattering theory

Reduction in intensity due to destructive interference of standing waves

Zachariasen: R = Q f(A)

R diffraction intensity
Q intensity per unit volume
f(A) diffraction geometry

$$A = \frac{e^2 \lambda F t}{m c^2 V}$$

λ wavelength
F structure factor
T nominal crystal/domain dimension
V unit cell volume

Neutron Time-of-Flight: refine extinction parameter via Sabine model (1985)

High-energy X-ray diffraction: no extinction???

Data Collection

Neutron Time-of-Flight

SEPD, IPNS

Exposed for 2 h at 13 µA and 30Hz, d-space range: 0.05 nm to 0.39 nm

25 keV X-ray

32 IDB, APS, eight detector machine, 0.8 mm spun kapton capillary

6° to 51° 2Θ, 0.0005° sw, 1 s ct, d-space range: 0.058 nm to 0.474 nm

67 keV X-ray

X17B1, NSLS, focusing optics, 1.0 mm spun glass capillary

2.7° to 12° 2Θ, 0.001° sw, 1 s ct, d-space range: 0.0890 nm to 0.393 nm

8 keV Laboratory X-ray

Siemens D500, Ge focusing IBM, sample spinner & PSD

20° to 154° 2Θ, 0.75° /min, d-space range: 0.079 nm to 0.44 nm

Data Analysis: Rietveld code GSAS

Minimize number of refined parameters

Four joint refinements

Constrain structural parameters across 24 specimens

Microstructural parameters constrained for alumina

Microstructural & extinction parameters constrained within each lot of silicon

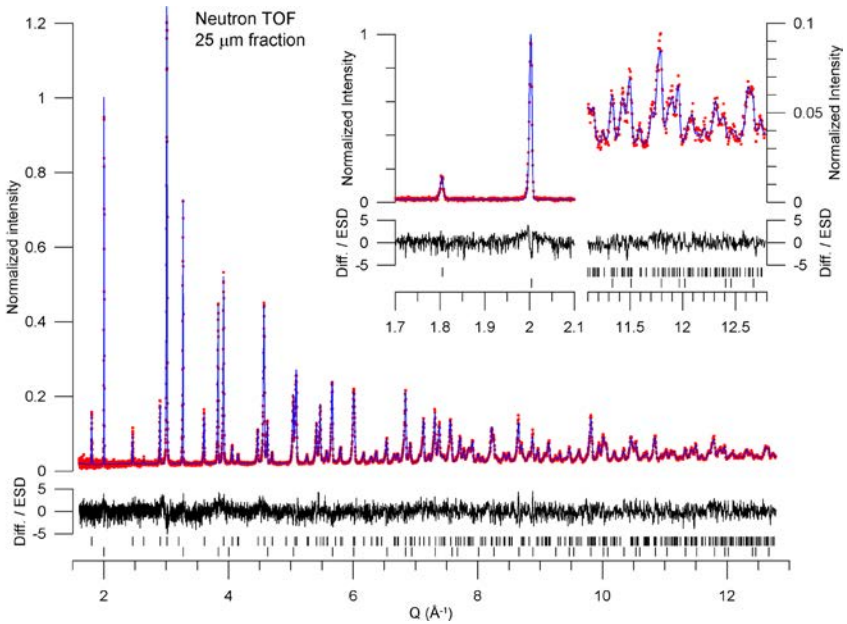

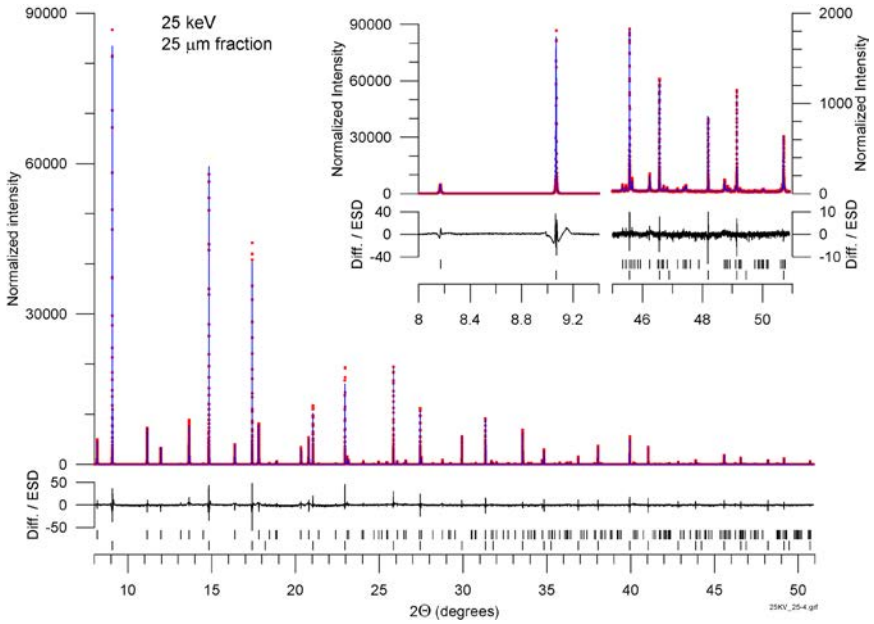

SRM 676a Certification Data

SRM 676a 99.02% ±1.11% phase pure alumina

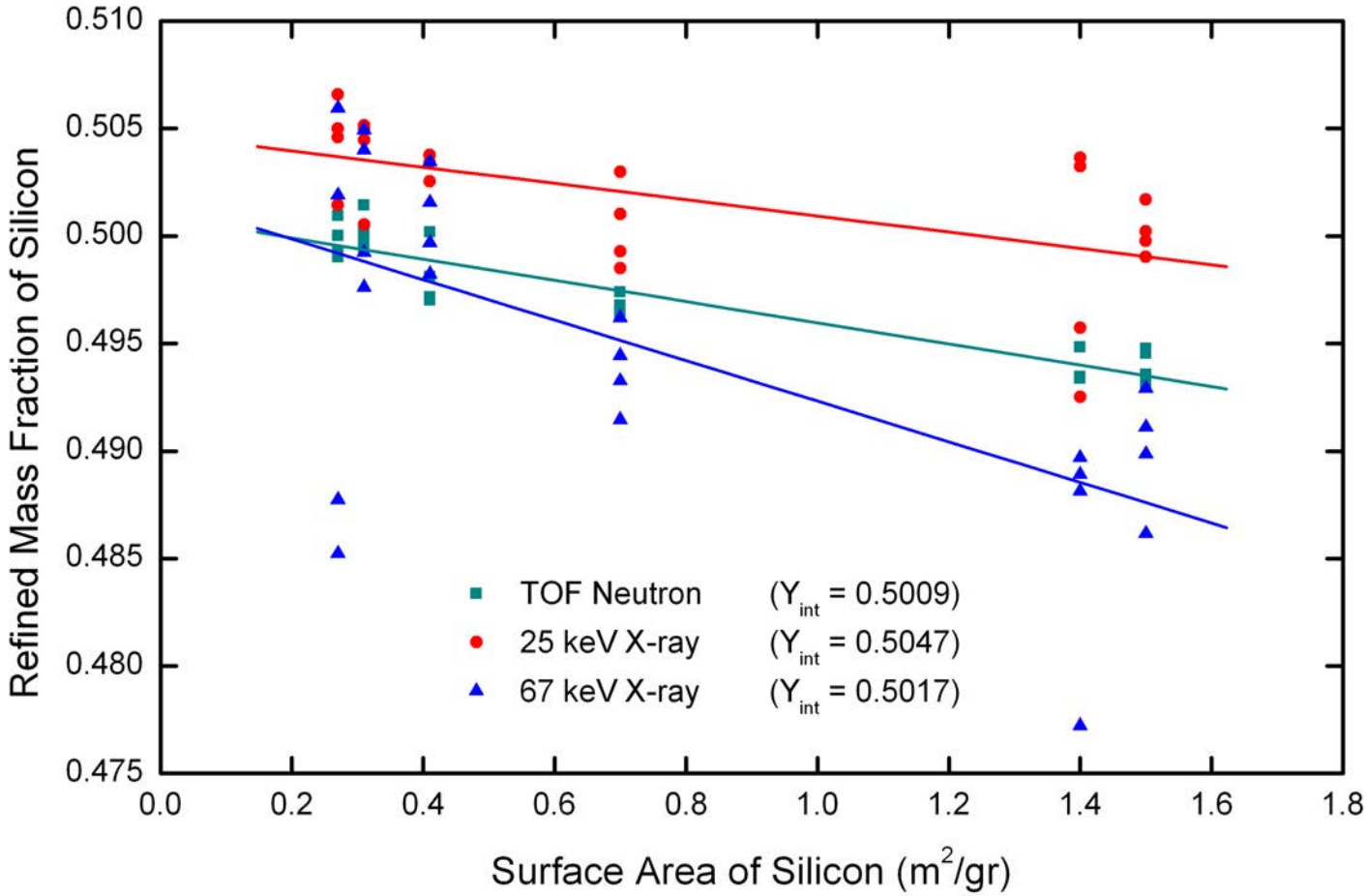

X-ray Data With / Without Extinction Correction

Extinction effects illustrated at < 5 μm particle size range & 67 keV

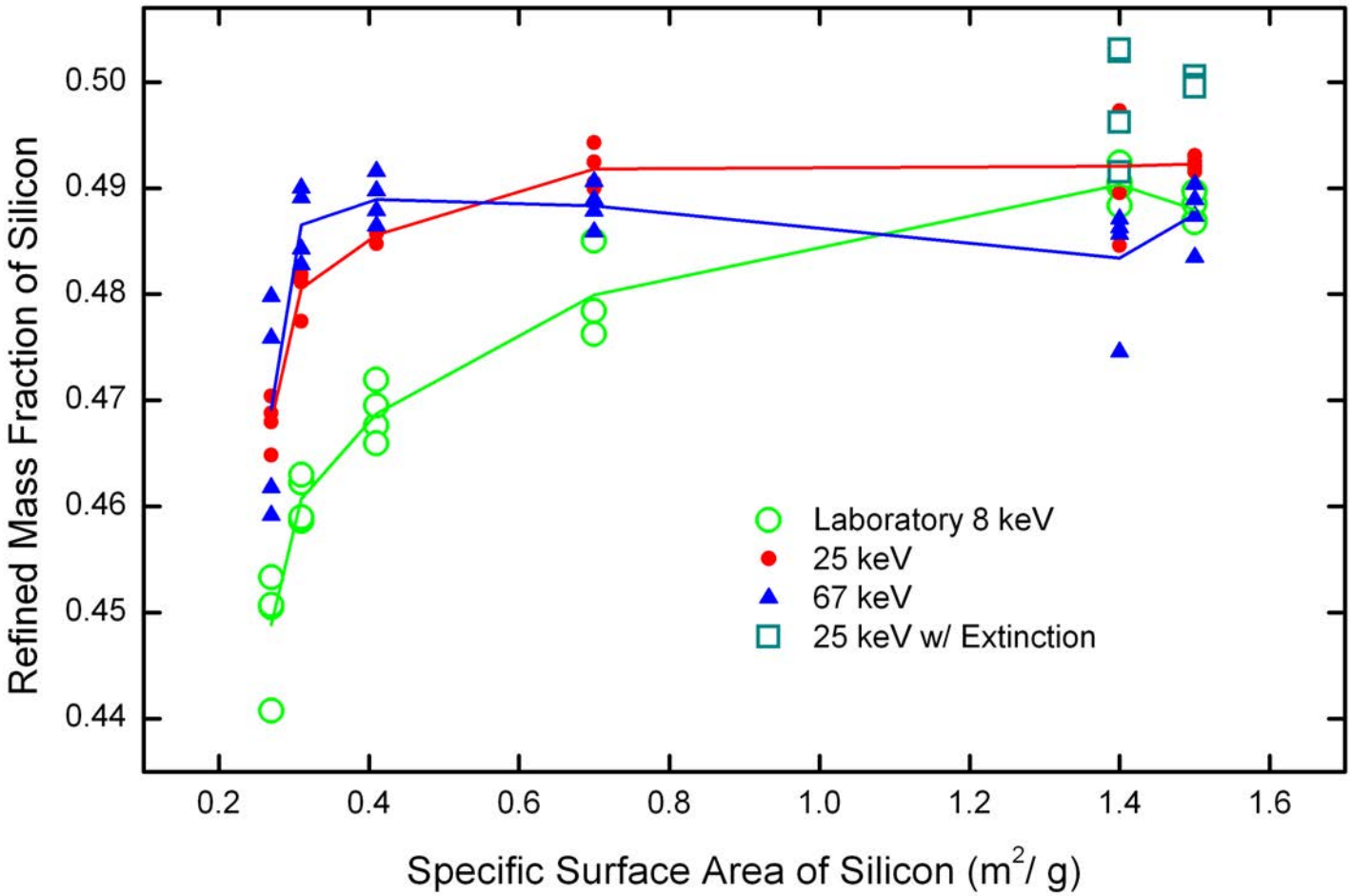

Refined Extinction Domain Sizes

Consistent within each method
Inconsistent between methods

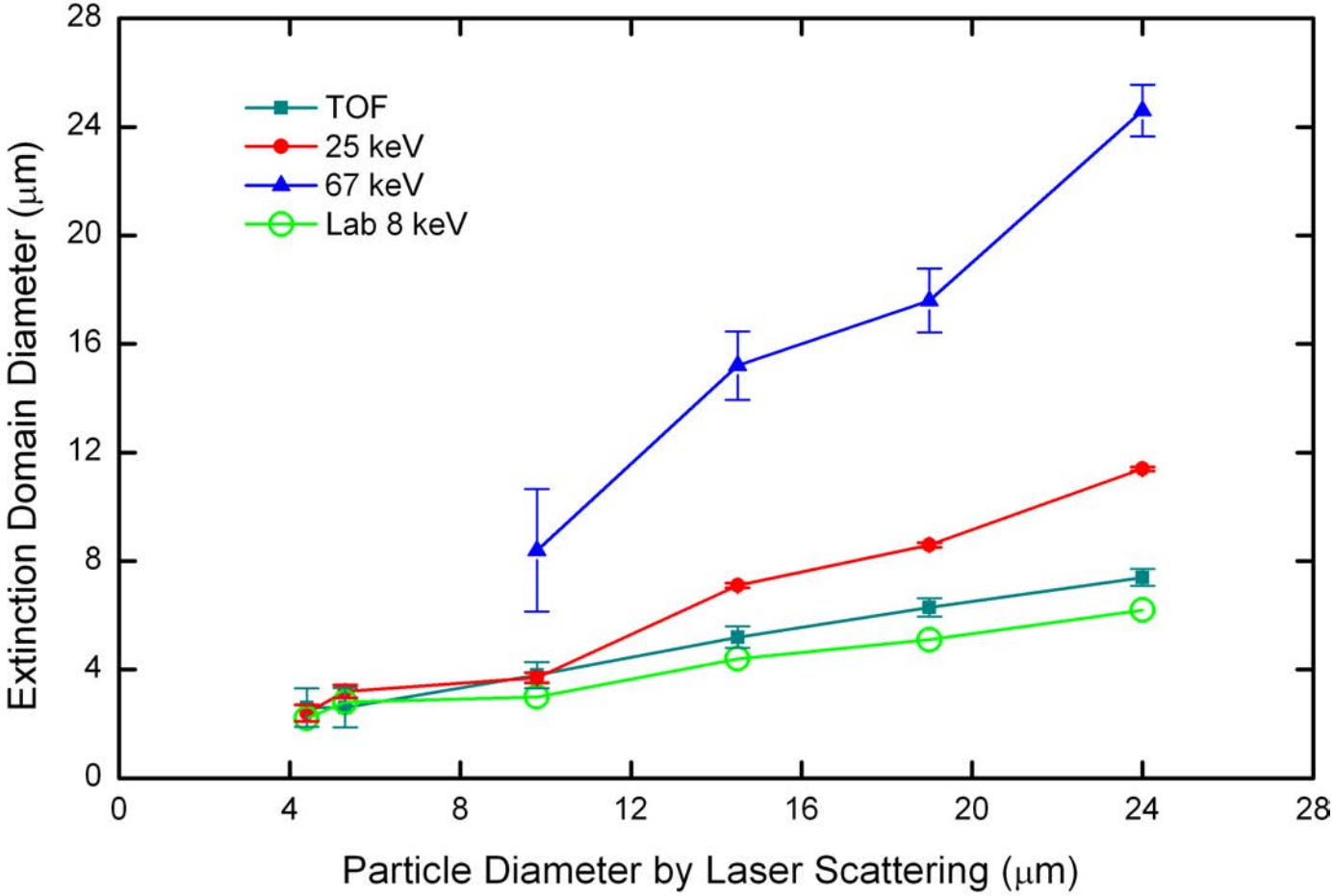

Thickness of Oxide (Gunk) Layer on Silicon Powder

Computed from line slope of certification data

Slope	=	Δ mass of Si displaced by SiO_2 / Δ surface area of Si
	=	0.0061 g/m^2 (average slope of TOF, 25 & 67 keV data sets)
Density of SiO_2	=	2.2 g/cm^3 = 0.45 cm^3/g
Layer thickness	=	0.0061 (g/m^2) * 0.45 (cm^3/g) * 10^{-6} (cm^3/m^3)
	=	0.0028 (cm^3/m^2) * 10^{-6} (cm^3/m^3)
Layer thickness	=	2.8 * 10^{-9} m = 2.8 nm

Generally accepted value for thickness of self-limiting oxide layer on silicon under ambient conditions is 1.5 nm

Conclusions

The divergent beam diffractometer has yielded lattice parameter values that are credible to ± 8 femtometers

We look forward to results from the parallel beam diffractometer

The *Fundamental Parameters Approach* yields the best fits to the observations and plausible refined parameters describing the experimental configuration

NIST quantitative analysis SRM 676a certified for amorphous content

SRM 676a now permits measurement
of layer thickness or amorphous content in unknowns

Extinction affects diffraction intensity measurements
with both small domain sizes and high energy radiation